

# Forecasting realized volatility in the stock market: a path-dependent perspective

Xiangdong Liu<sup>a</sup>, Sicheng Fu<sup>a</sup>, Shaopeng Hong<sup>b,\*</sup>

<sup>a</sup>*School of Economics, Jinan University, Guangzhou, 510000, China*

<sup>b</sup>*School of Statistics, Southwestern University of Finance and Economics, Chengdu, 610074, China*

---

## Abstract

Volatility forecasting in financial markets is a topic that has received more attention from scholars. In this paper, we propose a new volatility forecasting model that combines the heterogeneous autoregressive (HAR) model with a family of path-dependent volatility models (HAR-PD). The model utilizes the long- and short-term memory properties of price data to capture volatility features and trend features. By integrating the features of path-dependent volatility into the HAR model family framework, we develop a new set of volatility forecasting models. And, we propose a HAR-REQ model based on the empirical quartile as a threshold, which exhibits stronger forecasting ability compared to the HAR-REX model. Subsequently, the predictive performance of the HAR-PD model family is evaluated by statistical tests using data from the Chinese stock market and compared with the basic HAR model family. The empirical results show that the HAR-PD model family has higher forecasting accuracy compared to the underlying HAR model family. In addition, robustness tests confirm the significant predictive power of the HAR-PD model family.

*Keywords:* Volatility modeling, Path-dependence volatility, Realized volatility, HAR model family

---

## 1. Introduction

Volatility modeling has long been a key area of financial research. Traditionally, three types of models are considered: constant volatility models, local volatility models, and stochastic volatility models, e.g., (Black and Scholes, 1973; Dupire et al., 1994; Heston, 1993). However, constant volatility models and local volatility models have limitations in capturing the volatility smile phenomenon, making it difficult to model complex market dynamics effectively.

To address the limitations of traditional volatility models, Foschi and Pascucci (2008) introduced an innovative path-dependent volatility (PDV) model. This model captures the dependence of volatility on the asset's historical price path by incorporating a deviation process, thereby providing a more accurate depiction of market behavior. Furthermore, Fulvio and Roberto (2012) underscored the significant advantages of the PDV model in forecasting volatility.

By leveraging the entire historical trajectory of the underlying asset prices, the PDV model can more comprehensively capture long-term memory effects and complex dynamics, and remain highly sensitive to new market environments. The PDV model maintains forecast accuracy at different time scales and has a high sensitivity to extreme market events, which is particularly important for

---

\*Corresponding author

*Email addresses:* tliuxd@jnu.edu.cn (Xiangdong Liu), wangxiaobo018@stu.jnu.edu.cn (Sicheng Fu), Hong\_sp@outlook.com (Shaopeng Hong)

predicting potential large fluctuations. Parent (2022) integrated the concept of path dependence with the rough Heston model (Euch and Rosenbaum, 2018) to introduce the rough path-dependent volatility model. This model can capture a stronger Zumbach effect <sup>1</sup>. These research findings not only enrich the theoretical foundation of PDV models but also open up new avenues for their practical application in finance.

Guyon and Lekeufack (2023) pointed out that the predictive power of the PDV model for volatility lies in its ability to replicate the dynamic characteristics of volatility and provide a reinterpretation based on trend and volatility features. On the other hand, considering the volatility clustering phenomenon, a series of forecasting models have been proposed, such as the ARCH, GARCH, and its extensions, see e.g., (Engle, 1982; Glosten et al., 1993; Haas et al., 2004; Creal et al., 2013). However, these models have difficulty dealing with long-term dependencies and rely mainly on low-frequency data, which limits their ability to capture the dynamics of high-frequency trading activities.

To address this issue, Andersen and Bollerslev (1998) integrated realized volatility and constructed models such as the ARFIMA-RV suitable for high-frequency data, thereby improving volatility forecasting. Corsi (2009) pointed out the limitations of the model in capturing multi-scale dynamics. The HAR-RV model based on the heterogeneous market hypothesis solves this problem by integrating volatility components over different time horizons and significantly outperforms GARCH and ARFIMA-RV in financial volatility forecasting. Other scholars have further studied realized volatility and discovered another important aspect of volatility dynamics - jumps in intraday returns. These sudden and significant changes are called jumps, and point out that realized volatility can be decomposed into continuous and jump components. Lee and Mykland (2008) emphasized the key role of jumps in volatility modeling and its impact on accurate risk assessment and prediction. Lee and Mykland (2008) highlighted the significant importance of jumps in volatility modeling. Fulvio and Roberto (2012) further proposed the HAR model with jumps. To delve deeper into the jump process, Patton and Kevin (2015) assumed that the sign (positive or negative) of price jumps has different impacts on volatility. Using the realized semivariance estimator, Barndorff-Nielsen et al. (2008) decomposed realized volatility into positive semivariance and negative semivariance components. Clements and Rodrigo (2019), starting from the distribution characteristics of intraday returns, observed that during periods of financial turmoil, intraday returns may exhibit a heavy-tailed distribution, which affects volatility forecasting. Based on the tail distribution of returns, they defined extreme volatility and moderate volatility and proposed the HAR-REX model.

Synthesizing existing research discoveries, it has been demonstrated that high-frequency volatility models improved by methods such as jumps and realized semivariance (RS) can significantly enhance volatility forecasting accuracy. However, to date, no high-frequency volatility model has been constructed from the path-dependent perspective.

Based on the above discussion, this paper puts forward a novel volatility forecasting framework. It brings together the PDV model concept and the HAR model family structure. This integration aims to systematically consider the recent trajectory of asset prices to more comprehensively and accurately capture the dynamic characteristics of financial asset volatility.

The main contributions of our work are summarized as follows.

- (i) In this research, we demonstrate that the Chinese stock market possesses notable path-dependent

---

<sup>1</sup>The strong Zumbach effect refers to the phenomenon where the distribution of future realized volatility depends not only on past squared returns but also on the entire trajectory of past realized volatility. The weak Zumbach effect refers to the covariance between past squared returns and future realized volatility (within a given duration) being greater than the covariance between past realized volatility and future squared returns.

traits that are instrumental in explaining the underlying patterns of market volatility. Leveraging these insights, we have developed an innovative forecasting model designed to enhance the precision of stock market volatility predictions.

- (ii) Aiming to enhance predictive accuracy, we have refined the HAR-REX model by substituting the conventional cumulative normal distribution threshold with an innovative approach that employs empirical quartiles to re-segment realized volatility. Our empirical analyses reveal that the revamped HAR-REQ model, along with its extension, the HAR-PD-REQ model, exhibit significantly improved forecasting efficacy across daily, weekly, and monthly volatility horizons.
- (iii) Empirical results indicate that the HAR-PD model family, which is constructed based on path-dependent frameworks, exhibits superior predictive performance for forecasting realized volatility. The significance of the results persists even after undergoing various robustness tests, thereby confirming the reliability of the findings.

The remainder of this paper is structured as follows. In Section 2, we introduce the fundamental theories of volatility and the construction of volatility forecasting models. In Section 3, we present all the basic models used in this study and the methods for combining models. In Section 4, we discuss the volatility of the Chinese financial market from a path-dependent perspective and conduct an empirical analysis of the dataset. We use various statistical testing methods, including the Model Confidence Set (MCS) test (Hansen et al., 2011) and the out-of-sample  $R^2$  test (Campbell and Thompson, 2008), to evaluate the predictive capabilities of the HAR model family and the HAR-PD model family, and we report and discuss the results. In Section 5, we present the conclusion that the proposed HAR-PD model family demonstrates superior predictive ability.

## 2. Theoretical framework

Consider a complete filtered probability space  $(\Omega, \mathcal{F}, \{\mathcal{F}_t\}_{t \geq 0}, \mathbb{P})$ . The price  $S_t$  of a financial asset is assumed to follow the stochastic differential equation (SDE):

$$\frac{dS_t}{S_t} = \mu_t dt + \sigma_t dW_t + \kappa_t dq_t, \quad (1)$$

where  $\mu_t$  represents the drift term,  $\sigma_t$  denotes the instantaneous volatility,  $W_t$  is a standard Brownian motion,  $q_t$  is a Poisson counting process, and  $\kappa_t$  corresponds to the jump size.

Quadratic variation is a pivotal concept in stochastic process theory, serving as a sophisticated measure to characterize the volatility and variational behavior of random process trajectories. The integrated volatility  $IV_t$  represents the squared instantaneous volatility integrated over a time interval  $[0, T]$ . Integrated volatility is defined as:

$$IV_t = \int_0^t \sigma_s^2 ds,$$

when  $S_t$  does not contain jump components ( $\kappa_t = 0$ ), the quadratic variation is equal to the integrated volatility,

$$QV_t = IV_t = \int_0^t \sigma_s^2 ds.$$

However, when  $X_t$  contains jump components ( $\kappa_t \neq 0$ ), the quadratic variation is composed of both continuous and jump components, as shown by:

$$QV_t = \underbrace{\int_0^t \sigma_s^2 ds}_{\text{continuous component}} + \underbrace{\sum_{0 < s \leq t} \kappa_s^2}_{\text{jump component}} \neq IV_t.$$

Andersen and Bollerslev (1998) defined RV as the sum of squared intraday returns from high-frequency data, which is expressed as:

$$RV_t = \sum_{i=1}^n r_{t,i}^2 \xrightarrow{p} \int_0^t \sigma_s^2 ds + \sum_{0 < s \leq t} \kappa_s^2, \quad (2)$$

where  $r_{t,i} = \log S_{t,i} - \log S_{t,i-1}$  is the  $i$ -th log return on day  $t$ .  $S_{t,i}$  is the  $i$ -th log closing price on day  $t$ . They prove that under certain conditions, as the sampling frequency goes to infinity, realized volatility converges to the quadratic variation process in probability.

### 2.1. The PDV model

The PDV model assumes that the asset price  $S_t$  follows a functional SDE<sup>2</sup>:

$$\frac{dS_t}{S_t} = \mu_t dt + \sigma_t(S_u(u \leq t), G_t) dW_t, \quad (3)$$

where  $\mu_t$  denotes a progressively measurable stochastic process,  $W_t$  is a standard Brownian motion, and  $S_u(u \leq t)$  is the trajectory of  $S_u$  for 0 to  $t$ , representing a functional mapping from the sample space  $\mathbb{R}$  to the path space  $\mathcal{C}(\mathbb{R})$ . In contrast to classical jump-diffusion model (1), the PDV models (3) postulate that the volatility is dependent upon the entire trajectory of asset  $S_u(u \leq t)$  instead of  $S_t$ . This implies that the volatility is determined not only by the current price level but also by the path through which the price reaches its current level. The path-dependent variable  $G_t$  can incorporate various metrics, including the moving average ( $S_t^\Delta$ ), exponentially weighted moments ( $Y_t^\Delta$ ), and historical maximum or minimum prices ( $Max_t^\Delta$  and  $Min_t^\Delta$ ), where:

$$S_t^\Delta = \frac{\int_0^\Delta w_\tau S_{t-\tau} d\tau}{\int_0^\Delta w_\tau d\tau}, \quad Y_t^\Delta = \int_{-\infty}^\Delta \lambda e^{-\lambda(t-s)} \log \{S_t/S_s \cdot e^{-r(t-s)}\} ds,$$

$$Max_t^\Delta = \min_{t-\tau \leq u \leq t} S_u, \quad Min_t^\Delta = \min_{t-\tau \leq u \leq t} S_u.$$

Here,  $\Delta$  represents the time window length. For a one-day window,  $\Delta$  is set to 78, corresponding to the number of five-minute intervals in a typical 6.5-hour trading day ( $\Delta = 6.5 \times 60/5$ ). The term  $w_\tau$  in  $S_t^\Delta$  represents the weight function for time interval  $\tau$ , where  $w_\tau = 1$  corresponds to constant weights,  $w_\tau = \tau$  to linear weights, and  $w_\tau = e^{-\lambda\tau}$  to exponential weights, with  $\lambda > 0$  denoting the decay factor.

As demonstrated above, the PDV models establish that asset volatility is determined not only by current market conditions but also by the historical trajectory of asset prices. In other words, volatility dynamics are contingent upon past price movements, particularly the influence of historical volatility on current volatility levels. The fundamental premise of the model posits that market participants' behavior and market sentiment are significantly influenced by historical events. Through these inherent characteristics, the PDV models effectively capture volatility clustering, leverage effects, and asymmetric time-reversal properties via their explicit incorporation of historical price information, thereby enabling more accurate volatility predictions. To further elucidate the path-dependent properties of asset volatility, two key features have been developed: the trend feature  $R_{1,t}$  and the volatility feature  $R_{2,t}$ . The trend feature,  $R_{1,t}$ , characterizes the historical movement of asset

---

<sup>2</sup>The well-posedness of (3) has been extensively studied and is beyond the scope of this paper; interested readers may refer to Ning and Wu (2021) and Cozma and Reisinger (2018)

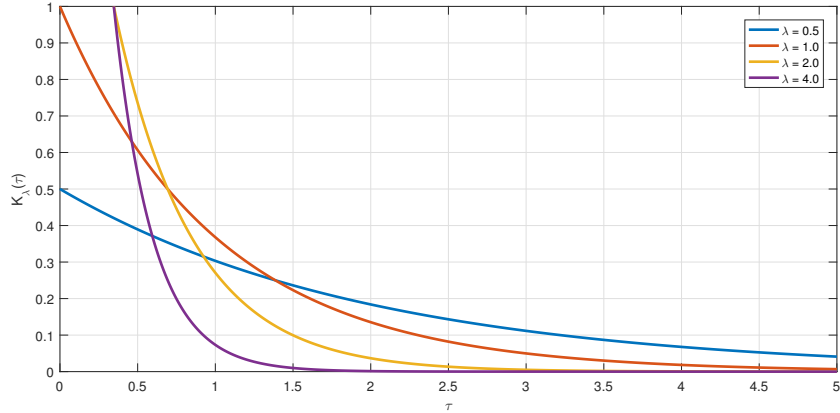


Figure 1 Exponential kernel function

prices, thereby reflecting long-term market trends, while the volatility feature measures historical price volatility levels, capturing short-term market fluctuations. Through the incorporation of these two features, the model comprehensively captures the dynamic evolution of asset volatility while accounting for market participants' reactions to historical events. The trend feature is constructed as a weighted sum of past returns, designed to capture the trend features of asset prices, expressed as:

$$R_{1,t} := \sum_{i < t} K_{\lambda_1}(t-i) \tilde{r}_{t-i}, \quad \tilde{r}_{t-i} = \frac{S_t - S_{t-i}}{S_{t-i}}, \quad (4)$$

where  $K_{\lambda_1}$  is a kernel function that assigns different weights to past daily returns based on the lag term  $t-i$ . Moreover,  $K_{\lambda_1}$  is specified as exponential kernels:

$$K_{\lambda}(\tau) = \lambda e^{-\lambda \cdot \tau}, \lambda > 0,$$

where the parameters  $\lambda$  determine the degree of influence past returns exert on current volatility.

As shown in Figure 1, the exponential kernel function decays differently across various  $\lambda$  values with respect to the time interval  $\tau$ . When  $\lambda = 4$ , the decay is most rapid, causing the model to prioritize recent returns while diminishing the influence of historical ones. Larger  $\lambda$  values reduce path dependency and reflect short-term dynamics, which is useful in fast-changing markets. In contrast, smaller  $\lambda$  values slow decay, allowing historical returns to significantly influence volatility and capturing long-memory effects, making them more suitable for markets with strong path dependency. Furthermore, the volatility characteristic, defined as the sum of squared past returns, is employed to capture recent price volatility and is expressed as:

$$R_{2,t} := \sum_{i < t} K_{\lambda_2}(t-i) \tilde{r}_{t-i}^2. \quad (5)$$

Guyon and Lekeufack (2023) demonstrated that the PDV models quantify volatility over time by incorporating trend and volatility features, thereby capturing both long-term and short-term effects. The fundamental model is expressed as:

$$RV_t = \beta_0 + \beta_1 R_{1,t} + \beta_2 R_{2,t} + \epsilon_t, \quad (6)$$

where  $\beta_0$  represents a constant term,  $\beta_1 \leq 0$  denotes the sensitivity parameter for the trend variable  $R_{1,t}$ , and  $\beta_2 \geq 0$  serves as the sensitivity parameter for  $R_{2,t}$ , which measures recent market price activity.

## 2.2. Realized volatility decomposition

### 2.2.1. Continuous and discrete components

Barndorff-Nielsen and Shephard (2004) introduced the realized bipower variation (RBV<sub>t</sub>), and under certain conditions, they proved that RBV<sub>t</sub> is a consistent estimator of the integrated volatility. The expression for RBV<sub>t</sub> is given as follows:

$$\text{RBV}_t = \frac{n}{\mu_1^2(n-1)} \sum_{i=2}^n |r_{t,i-1}| |r_{t,i}|,$$

where  $\mu_1 = \sqrt{2/\pi}$ , and the factor  $n/(n-1)$  is used to adjust for sample size. Barndorff-Nielsen and Shephard (2003) demonstrated that under the assumption that the price process  $S_t$  is a semimartingale, RBV<sub>t</sub> serves as a consistent estimator of the integrated volatility and the difference between RV<sub>t</sub> and RBV<sub>t</sub> provides an estimator for jump variation.

$$\text{RBV}_t \xrightarrow{p} \int_0^t \sigma_s^2 ds, \quad \text{and} \quad \text{RV}_t - \text{RBV}_t \xrightarrow{p} \sum_{0 < s \leq t} \kappa_s^2.$$

Moreover, Huang and Tauchen (2005) proposed a  $Z$ -statistic for jump identification and to remove the influence of these insignificant jumps. The  $Z$ -statistic is defined as:

$$Z_t = \frac{\sqrt{n}(\text{RV}_t - \text{RBV}_t)\text{RV}_t^{-1}}{\sqrt{(\mu_1^{-4} + 2\mu_1^{-2} - 5) \max\left(1, \frac{\text{RTQ}_t}{\text{RBV}_t^2}\right)}},$$

where RTQ<sub>t</sub> is the realized tripower quarticity, given by:

$$\text{RTQ}_t = \frac{n^2}{\mu_{4/3}^3(n-4)} \sum_{k=5}^n |r_{t,k-4}|^{4/3} \cdot |r_{t,k-2}|^{4/3} \cdot |r_{t,k}|^{4/3},$$

where  $\mu_{4/3} = 2^{2/3}\Gamma(1/6)/(6\pi^{1/2})$ . Based on the properties of this indicator function, the significant jumps can be isolated:

$$\text{CJ}_{t,\alpha} = I(Z_t > \phi_{1-\alpha})(\text{RV}_t - \text{RBV}_t),$$

where  $I(\cdot)$  is indicator function,  $\phi_{1-\alpha}$  is the  $(1-\alpha)$ -quantile of the standard normal distribution. Here  $\alpha$  is set to 0.05 and is used in the rest of the paper.

### 2.2.2. Realized semivariance

Barndorff-Nielsen et al. (2008) posited that, in financial markets, downside risk is typically more significant than upside risk for most investors, as it directly relates to potential losses. Based on this observation, the realized semivariance is introduced as a novel risk measure, focusing on capturing price fluctuations during periods of negative returns. Realized semivariance distinguishes between positive and negative intraday logarithmic returns and calculates the sum of squared positive intraday logarithmic returns to derive both positive and negative semivariance. The expression is as follows:

$$\text{RS}_t^- = \sum_{i=1}^n r_{t,i}^2 I(r_{t,i} < 0), \quad \text{RS}_t^+ = \sum_{i=1}^n r_{t,i}^2 I(r_{t,i} > 0).$$

### 2.2.3. Extreme and moderate volatility

Extreme events in financial markets, such as financial crises, large-scale market crashes, and circuit breakers, can significantly impact volatility. These events often lead to dramatic changes in market volatility over a short period, which traditional volatility measures may fail to capture effectively. Furthermore, market volatility exhibits dynamic multiscale characteristics, meaning both short-term and long-term volatility components coexist. Traditional volatility measures and forecasting models may not adequately capture this multiscale nature, particularly the long-term component's impact. To address these issues, [Clements and Rodrigo \(2019\)](#) proposed a new decomposition method, which divides realized volatility into moderate and extreme realized volatility. The procedure is as follows:

- (i) **Threshold determination:** For daily time  $t$ , calculate the unconditional volatility  $\sigma_t$  of the daily return, where  $t = 1, 2, \dots, N$ ,  $N$  is the number of days. Then choose the tail probability  $\alpha$ , and define the positive and negative thresholds according to this probability as:

$$r_t^- = F^{-1}(\alpha)\sigma_t, \quad r_t^+ = F^{-1}(1 - \alpha)\sigma_t,$$

where  $F^{-1}$  is the inverse cumulative distribution function of the normal distribution.

- (ii) **Moderate Realized Volatility Construction:** The moderate realized volatility ( $\text{REX}_t^m$ ) is calculated by squaring the returns for each period and summing those that lie between the positive and negative thresholds. Specifically, a threshold is set for each day  $t$  and if  $r_t^- \leq r_{t,i} \leq r_t^+$ , the squared return  $r_{t,i}^2$  is added to the moderate volatility construction:

$$\text{REX}_t^m = \sum_{i=1}^n r_{t,i}^2 I(r_t^- < r_{t,i} < r_t^+).$$

- (iii) **Extreme Volatility Construction:** Extreme volatility is divided into positive extreme realized volatility,  $\text{REX}_t^+$ , and negative extreme realized volatility,  $\text{REX}_t^-$ . A threshold is set for each day  $t$  and if  $r_{t,i} \geq r_t^+$ , the squared return  $r_{t,i}^2$  is added to the positive extreme volatility construction; if  $r_{t,i} \leq r_t^-$ , it is added to the negative extreme volatility construction:

$$\text{REX}_t^- = \sum_{i=1}^n r_{t,i}^2 I(r_{t,i} \leq r_t^-), \quad \text{REX}_t^+ = \sum_{i=1}^n r_{t,i}^2 I(r_{t,i} \geq r_t^+).$$

Using this method, volatility is decomposed into three components: moderate volatility ( $\text{REX}_t^m$ ), which captures the long-term component; positive extreme volatility ( $\text{REX}_t^+$ ), and negative extreme volatility ( $\text{REX}_t^-$ ), which together capture the short-term component.

The positive and negative thresholds are defined by selecting the tail probability  $\alpha$ . Subsequently, the positive and negative thresholds are set as  $r_t^- = F^{-1}(\alpha)\sigma_t$  and  $r_t^+ = F^{-1}(1 - \alpha)\sigma_t$ , based on which extreme and moderate volatility are computed. [Clements and Rodrigo \(2019\)](#) sets  $F^{-1}$  as the CDF of the standard normal distribution, but financial returns often exhibit the characteristics of leptokurtosis, heavy-tailed distributions, or asymmetry. We suggest using empirical quantile to replace  $F^{-1}(\alpha)\sigma_t$ . The 0.95 quantile is taken as the positive threshold, with the portion of intraday returns exceeding this threshold designated as extreme positive volatility. Similarly, the 0.05 quantile is taken as the negative threshold, with the portion of intraday returns below this threshold designated as extreme negative volatility. The portion between the positive and negative



thresholds is classified as moderate volatility. The expressions are given as follows:

$$\begin{aligned}\text{REXQ}_t^- &= \sum_{i=1}^n r_{t,i}^2 I(r_{t,i} \leq \hat{Q}_{t,0.05}), \\ \text{REXQ}_t^+ &= \sum_{i=1}^n r_{t,i}^2 I(r_{t,i} \geq \hat{Q}_{t,0.95}), \\ \text{REXQ}_t^m &= \sum_{i=1}^n r_{t,i}^2 I(\hat{Q}_{t,0.05} < r_{t,i} < \hat{Q}_{t,0.95}).\end{aligned}$$

Where  $\hat{Q}_{t,0.05}$  is based on the actual returns within each trading day  $t$  to determine the thresholds for extreme and moderate volatility, thereby providing a basis for the decomposition of volatility. The construction HAR-REQ is applied in (10).

### 3. Volatility prediction models

#### 3.1. Benchmark: HAR model family

Drawing upon the heterogeneous market hypothesis, [Corsi \(2009\)](#) developed a model that integrates realized volatility across multiple time scales to capture both long-term and short-term volatility dynamics in financial markets, expressed as:

$$\text{RV}_t = \beta_0 + \beta_1 \text{RV}_{t-1} + \beta_2 \overline{\text{RV}}_{t-5} + \beta_3 \overline{\text{RV}}_{t-22} + \epsilon_t. \quad (7)$$

The model comprises three explanatory variables:  $\text{RV}_{t-1}$ ,  $\overline{\text{RV}}_{t-5}$ , and  $\overline{\text{RV}}_{t-22}$ , which correspond to short-term (daily), medium-term (weekly), and long-term (monthly) volatility, respectively. The coefficients  $\beta_0, \beta_1, \beta_2, \beta_3$  in (7) can be estimated using the loss function MSE for estimation. The lagged terms  $\overline{\text{RV}}_{t-5}$  and  $\overline{\text{RV}}_{t-22}$  represent 5-step and 22-step lags, respectively, and can be generalized as  $\overline{\text{RV}}_{t-h}$ , where  $h$  denotes the number of lag terms, calculated as:

$$\overline{\text{RV}}_{t-h} = \frac{1}{h} (\text{RV}_{t-1} + \dots + \text{RV}_{t-h}). \quad (8)$$

[Andersen et al. \(2007\)](#) and [Corsi and Reno \(2009\)](#) developed a new HAR model through the decomposition of continuous and jump volatility components. The model is constructed as follows:

$$\text{RV}_t = \beta_0 + \beta_1 \text{CV}_{t-1} + \beta_2 \overline{\text{CV}}_{t-5} + \beta_3 \overline{\text{CV}}_{t-22} + \beta_4 \text{CJ}_{t-1} + \beta_5 \overline{\text{CJ}}_{t-5} + \beta_6 \overline{\text{CJ}}_{t-22} + \epsilon_t,$$

where  $\text{CV}_{t-1}$  and  $\text{CJ}_{t-1}$  denote the first-order lags of  $\text{CV}_t$  and  $\text{CJ}_t$ , respectively. The terms  $\overline{\text{CV}}_{t-5}$ ,  $\overline{\text{CV}}_{t-22}$ ,  $\overline{\text{CJ}}_{t-5}$ , and  $\overline{\text{CJ}}_{t-22}$  are constructed similarly to (8).

Drawing upon realized semivariance, [Patton and Kevin \(2015\)](#) introduced the HAR-RS model, which incorporates both positive and negative semivariance components:

$$\text{RV}_t = \beta_0 + \beta_1 \text{RS}_{t-1}^+ + \beta_2 \overline{\text{RS}}_{t-5}^+ + \beta_3 \overline{\text{RS}}_{t-22}^+ + \beta_4 \text{RS}_{t-1}^- + \beta_5 \overline{\text{RS}}_{t-5}^- + \beta_6 \overline{\text{RS}}_{t-22}^- + \epsilon_t.$$

[Clements and Rodrigo \(2019\)](#) proposed the HAR-REX model by incorporating extreme volatility and bidirectional moderate volatility components:

$$\begin{aligned}\text{RV}_t = \beta_0 + \beta_1 \text{REX}_{t-1}^+ + \beta_2 \overline{\text{REX}}_{t-5}^+ + \beta_3 \overline{\text{REX}}_{t-22}^+ + \beta_4 \text{REX}_{t-1}^- + \beta_5 \overline{\text{REX}}_{t-5}^- + \\ \beta_6 \overline{\text{REX}}_{t-22}^- + \beta_7 \text{REX}_{t-1}^m + \beta_8 \overline{\text{REX}}_{t-5}^m + \beta_9 \overline{\text{REX}}_{t-22}^m + \epsilon_t,\end{aligned} \quad (9)$$



where the construction of variables in (9) is similar to that in (8).

The HAR-REQ model is constructed using empirical quantiles and can be expressed as follows:

$$\begin{aligned} RV_t = & \beta_0 + \beta_1 \text{REQ}_{t-1}^+ + \beta_2 \overline{\text{REQ}}_{t-5}^+ + \beta_3 \overline{\text{REQ}}_{t-22}^+ + \beta_4 \text{REQ}_{t-1}^- + \beta_5 \overline{\text{REQ}}_{t-5}^- + \\ & \beta_6 \overline{\text{REQ}}_{t-22}^- + \beta_7 \text{REQ}_{t-1}^m + \beta_8 \overline{\text{REQ}}_{t-5}^m + \beta_9 \overline{\text{REQ}}_{t-22}^m + \epsilon_t, \end{aligned} \quad (10)$$

where  $\text{REQ}_{t-1}^-$ ,  $\overline{\text{REQ}}_{t-5}^-$ , and  $\overline{\text{REQ}}_{t-22}^-$  represent the negative extreme volatility based on daily, weekly, and monthly empirical quantiles, respectively. The other components are denoted in a similar manner.

### 3.2. Encoding path-dependent: HAR-PD models

The structure of (6) from Section 2.1 is incorporated into the HAR model family to construct the HAR-PD model family. As established in Section 2.1, it is clear that  $R_{2,t}$  as a volatility feature is more explanatory of realized volatility, along with the structure of the trend feature  $R_{1,t}$ . The HAR-RV model is restructured by incorporating path dependence to form the HAR-PD-RV model:

$$RV_t = \beta_0 + \beta_1 R_{2,t-1} + \beta_2 \overline{R}_{2,t-5} + \beta_3 \overline{R}_{2,t-22} + \epsilon_t,$$

where  $R_{2,t-1}$ ,  $\overline{R}_{2,t-5}$ , and  $\overline{R}_{2,t-22}$  represent volatility features based on the moments  $t-1$ ,  $t-5$ , and  $t-22$ , respectively. The construction method for  $\overline{R}_{2,t-h}$  is similar (5).

Considering the decomposition of jump and continuous components, the HAR-PD-CJ model is formulated as follows:

$$\begin{aligned} RV_t = & \beta_0 + \beta_1 R_{2,t-1} + \beta_2 \overline{R}_{2,t-5} + \beta_3 \overline{R}_{2,t-22} + \beta_4 \text{PDCJ}_{t-1} + \beta_5 \overline{\text{PDCJ}}_{t-5} + \\ & \beta_6 \overline{\text{PDCJ}}_{t-22} + \beta_7 \text{PDCV}_{t-1} + \beta_8 \overline{\text{PDCV}}_{t-5} + \beta_9 \overline{\text{PDCV}}_{t-22} + \epsilon_t. \end{aligned} \quad (11)$$

The construction method of  $\overline{\text{PDCJ}}_{t-h}$  can be found in (8).

In the HAR-PD-CJ model, the volatility characteristics incorporate both jump and continuous components. The volatility characteristics describe the overall fluctuation within a specific time period, while jumps in financial markets indicate significant changes in asset prices. By incorporating jump characteristics, volatility predictions can be improved, particularly for fluctuations caused by public events, announcements, and other market uncertainties. Here,  $\text{PDCJ}_{t-1}$ ,  $\overline{\text{PDCJ}}_{t-5}$ , and  $\overline{\text{PDCJ}}_{t-22}$  represent the jump components based on the path dependence at time  $t-1$ ,  $t-5$ ,  $t-22$  respectively. Combined with the constructor of (4), the  $\text{PDCJ}_t$  can be constructed as:

$$\text{PDCJ}_t = \sum_{i < t} K_\lambda(t-i) \text{CJ}_{t-i}. \quad (12)$$

Considering the decomposition of positive and negative variance, the HAR-PD-RS model is formulated as follows:

$$\begin{aligned} RV_t = & \beta_0 + \beta_1 R_{1,t-1} + \beta_2 \overline{R}_{1,t-5} + \beta_3 \overline{R}_{1,t-22} + \beta_4 \text{PDRS}_{t-1}^+ + \beta_5 \overline{\text{PDRS}}_{t-5}^+ + \\ & \beta_6 \overline{\text{PDRS}}_{t-22}^+ + \beta_7 \text{PDRS}_{t-1}^- + \beta_8 \overline{\text{PDRS}}_{t-5}^- + \beta_9 \overline{\text{PDRS}}_{t-22}^- + \epsilon_t. \end{aligned}$$

The basic HAR-RS model decomposes the realized semivariance into positive and negative components for volatility prediction. This decomposition captures both the actual price skewness within specific time periods and the dynamic evolution of realized skewness, thereby providing insights into volatility patterns. The construction method for  $\text{PDRS}_t$  is shown in (12), and the construction methods for  $\overline{\text{PDRS}}_{t-h}^+$  and  $\overline{\text{PDRS}}_{t-h}^-$  are shown in (8).

The HAR-PD-REX model, based on the cumulative distribution function of the normal distribution and involving the decomposition of volatility into extreme and moderate components, is formulated as follows:

$$\begin{aligned} RV_t = & \beta_0 + \beta_1 R_{1,t-1} + \beta_2 \bar{R}_{1,t-5} + \beta_3 \bar{R}_{1,t-22} + \beta_4 \text{PDREX}_{t-1}^+ + \beta_5 \overline{\text{PDREX}}_{t-5}^+ + \\ & \beta_6 \overline{\text{PDREX}}_{t-22}^+ + \beta_7 \text{PDREX}_{t-1}^- + \beta_8 \overline{\text{PDREX}}_{t-5}^- + \beta_9 \overline{\text{PDREX}}_{t-22}^- + \\ & \beta_{10} \text{PDREX}_{t-1}^m + \beta_{11} \overline{\text{PDREX}}_{t-5}^m + \beta_{12} \overline{\text{PDREX}}_{t-22}^m + \epsilon_t, \end{aligned}$$

where, the construction methods of  $\text{PDREX}_{t-1}^+$ ,  $\text{PDREX}_{t-1}^-$ , and  $\text{PDREX}_{t-1}^m$  are similar to (12).

The HAR-PD-REQ model is constructed based on the method of empirical quantiles as follows:

$$\begin{aligned} RV_t = & \beta_0 + \beta_1 R_{1,t-1} + \beta_2 \bar{R}_{1,t-5} + \beta_3 \bar{R}_{1,t-22} + \beta_4 \text{PDREQ}_{t-1}^+ + \beta_5 \overline{\text{PDREQ}}_{t-5}^+ + \\ & \beta_6 \overline{\text{PDREQ}}_{t-22}^+ + \beta_7 \text{PDREQ}_{t-1}^- + \beta_8 \overline{\text{PDREQ}}_{t-5}^- + \beta_9 \overline{\text{PDREQ}}_{t-22}^- + \\ & \beta_{10} \text{PDREQ}_{t-1}^m + \beta_{11} \overline{\text{PDREQ}}_{t-5}^m + \beta_{12} \overline{\text{PDREQ}}_{t-22}^m + \epsilon_t. \end{aligned}$$

The construction methods of  $\text{PDREQ}_{t-1}^+$ ,  $\overline{\text{PDREQ}}_{t-5}^+$ , and  $\overline{\text{PDREQ}}_{t-22}^+$  are similar to those of (8) and (12).

### 3.2.1. Shrinkage: LASSO-HAR-PD models

The introduction of path-dependent features, while enhancing the predictive capability of models, may also lead to an increase in the number of model parameters, thereby causing overfitting. To demonstrate that the enhancement of predictive performance is not solely due to an increase in the number of variables, several strategies have been proposed by researchers. For instance, [Ding et al. \(2021\)](#) and [Audrino and Knaus \(2016\)](#) suggested incorporating LASSO ([Tibshirani, 1996](#)) into the model to control the number of parameters, thereby effectively preventing overfitting. Additionally, [Burnham and Anderson \(2004\)](#) proposed that the complexity of models could be assessed by incorporating information criteria (such as AIC and BIC), and these criteria could be used to compare the predictive accuracy of models, thereby further elucidating the balance between model complexity and predictive performance. Write  $\boldsymbol{\beta} = (\beta_1, \dots, \beta_d)^\top$ . Suppose the sample size is  $N$ , the loss function of LASSO-HAR-PD models can be written as:

$$\mathcal{L}(\boldsymbol{\beta}) = \frac{1}{2} \sum_{t=1}^N (RV_t - \mathbf{X}_t^\top \boldsymbol{\beta})^2 + \lambda \sum_{j=1}^p |\beta_j|.$$

where  $\lambda$  is the tuning parameters we selecting by 10-fold validation, and  $\mathbf{X}_t$  is a vector that comprises the covariates of interest. For instance, in (11),  $\mathbf{X}_t = (R_{2,t-1}, \bar{R}_{2,t-5}, \bar{R}_{2,t-22}, \overline{\text{PDCJ}}_{t-5}, \overline{\text{PDCV}}_{t-5})^\top$ .

## 4. Empirical analysis

### 4.1. The Path-dependency property of realized volatility

In order to argue that the Chinese stock market is also characterized by path-dependence, we compare a path-dependence model that includes the historical price paths of stocks with a non-path-dependence model that assumes that price movements are independent of past paths. The data used are from the Wind database. Considering the non-negligible microstructure noise in the commodity market ([Ait-Sahalia et al., 2005](#); [Zhang et al., 2005](#)), five-minute high-frequency data are selected as suggested by [Corsi et al. \(2008\)](#). The datasets include the SSE (000001), CSI 300 (000300), SSE

50 (000016), GEI (399006), SSE 50 ETF (510050), and STAR 50 (000688). The SSE covers the period from January 4, 2005, to December 29, 2023. The SSE 50 covers the same period. The CSI 300 covers the period from April 8, 2005, to December 29, 2023. The GEI covers the period from June 1, 2010, to December 29, 2023. The SSE 50 ETF covers the period from February 23, 2005, to December 29, 2023. The STAR 50 covers the period from July 23, 2020, to December 29, 2023. The realized volatility model based on the path dependence property is constructed as follows:

$$RV_t = \beta_0 + \beta_1 R_{1,t} + \beta_2 R_{2,t} + \epsilon_t. \quad (13)$$

Consider a volatility model that lacks path-dependent properties, specifically one without an exponential kernel function:

$$RV_{t,null} = \beta_0 + \beta_1 r_t + \beta_2 r_t^2 + \epsilon_t. \quad (14)$$

In this context, (14) denotes the method for calculating returns based on non-path-dependence, where  $r_t$  is defined by (4). Meanwhile, the power kernel function  $K_\lambda(\tau)$  is chosen to compute (13).

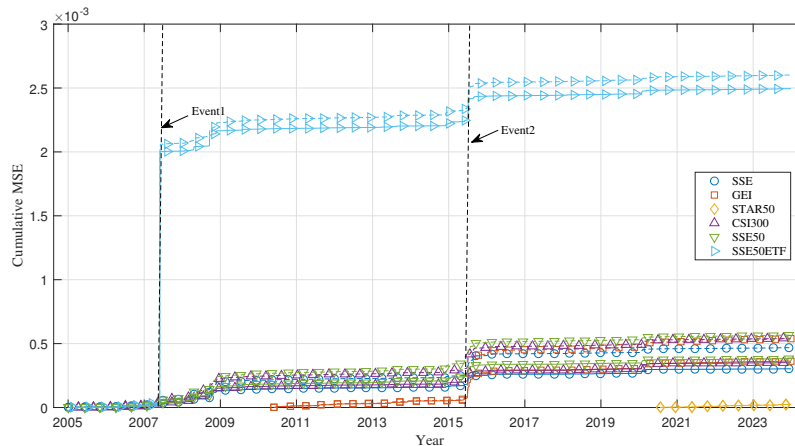


Figure 2 Cumulative mean square error of realized volatility and path-dependent characteristics

Table 1 reports the parameter estimates of the path-dependent and non-path-dependent models under high-frequency data for the Chinese stock market. The trend feature ( $R_{1,t}$ ) and volatility feature ( $R_{2,t}$ ) used in the path-dependent model are constructed based on the historical price paths of assets. The parameter estimation results show that the adjusted  $R^2$  of the path-dependent model is much higher than the adjusted  $R^2$  of the non-path-dependent model under all data, compared to the non-path-dependent model, which assumes that price changes are independent of past paths. Among them, the lowest goodness of fit is  $RV_{null}^{050}$  and the highest is  $RV^{001}$ .

In order to visualize the path-dependent characteristics of the Chinese stock market, Figure 2 shows the cumulative mean-square error of realized volatility (13) constructed based on the path-dependent characteristics and the realized volatility (14) of the non-path-dependent characteristics (without index kernel function) in the Chinese stock market in comparison, respectively. The data used include SSE (000001), CSI 300 (000300), SSE 50 (000016), GEI (399006), SSE 50 ETF (510050), and STAR 50 (000688). Where the horizontal axis indicates time and the vertical axis indicates mean square error. All solid lines denote the cumulative mean-squared error of the realized volatility constructed by path dependence, and all dashed lines denote the cumulative mean-squared error of the realized volatility constructed by non-path dependence. The black dashed line in the figure indicates the time period when the cumulative mean-squared error of each stock shows abnormal fluctuations.

Table 1 Results of parameter estimation with and without path-dependence for each index

Non-path-dependent parameter estimates						
	$\lambda_1$	$\lambda_2$	$\beta_0$	$\beta_1$	$\beta_2$	$Adj.R^2$
$RV_{null}^{001}$			0.000** (0.000)	-0.001*** (0.000)	0.385*** (0.008)	0.352
$RV_{null}^{50}$			0.000*** (0.000)	-0.000* (0.000)	0.378*** (0.007)	0.343
$RV_{null}^{300}$			0.000*** (0.000)	-0.001*** (0.000)	0.367*** (0.007)	0.334
$RV_{null}^{006}$			0.000*** (0.000)	-0.002*** (0.000)	0.312*** (0.010)	0.245
$RV_{null}^{050}$			0.000*** (0.000)	-0.000 (0.000)	0.397*** (0.015)	0.129
$RV_{null}^{688}$			0.000*** (0.000)	-0.000 (0.000)	0.145*** (0.012)	0.129
Path-dependent parameter estimates						
	$\lambda_1$	$\lambda_2$	$\beta_0$	$\beta_1$	$\beta_2$	$Adj.R^2$
$RV^{001}$	0.534*** (0.000)	0.520*** (0.060)	0.000*** (0.000)	-0.005*** (0.032)	0.778*** (0.125)	0.581
$RV^{50}$	0.432*** (0.000)	0.408 (0.173)	0.00*** (0.000)	-0.002*** (0.000)	0.825*** (0.010)	0.573
$RV^{300}$	0.731*** (0.000)	0.326*** (0.057)	0.000 (0.000)	-0.003*** (0.000)	0.852*** (0.015)	0.565
$RV^{006}$	0.838*** (0.000)	0.453*** (0.003)	0.000 (0.000)	-0.006** (0.000)	0.742*** (0.098)	0.518
$RV^{050}$	0.809*** (0.000)	0.644*** (0.005)	0.000 (0.000)	-0.002* (0.001)	0.790*** (0.022)	0.221
$RV^{688}$	0.571*** (0.001)	0.649*** (0.005)	0.000* (0.000)	-0.001* (0.000)	0.310*** (0.019)	0.235

Note:  $Adj.R^2$  denotes the adjusted goodness-of-fit. \*, \*\*, \*\*\* denote the rejection of the original hypothesis at 10%, 5% and 1% significance levels, standard deviation of each parameter is shown in parentheses, and all estimation results are retained to three decimal places.

Event 1: At that time, the Chinese stock market experienced an unprecedented 'bull market'. This volatility was primarily driven by strong economic growth and increased global capital flows, leading to a sharp rise in investor optimism, which pushed market valuations to extremely high levels. This optimism reflected market participants' positive expectations for future economic prospects and a general confidence in sustained growth potential.

Event 2: From early 2015 to mid-June, the Chinese stock market rose rapidly, with the Shanghai Composite Index and Shenzhen Component Index achieving gains beyond predictions, mainly driven by retail investors who were significantly influenced by leveraged funds. However, as a market bubble formed and regulatory policies were implemented, the stock

market began to plummet sharply after mid-June, resulting in significant market volatility. In response to the rapid market decline, the government implemented a series of intervention measures, including suspending IPOs, implementing a circuit breaker mechanism, and deploying the 'national team' to stabilize the market.

By analyzing Events 1 and 2, we find that the model with path-dependent characteristics is able to accurately fit the market volatility. As shown in Figure 2, the path-dependent model utilizing past price path information exhibits a smaller prediction error than the model with non-path-dependent characteristics, and this difference is statistically significant. Overall, the empirical results confirm the validity of the path-dependent model in the Chinese stock market, with a high degree of fit between the model and the actual volatility.

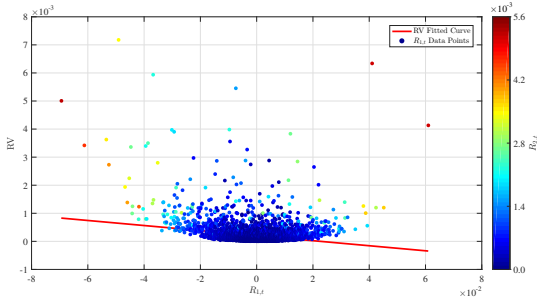


Figure 3 Realized volatility and trend features

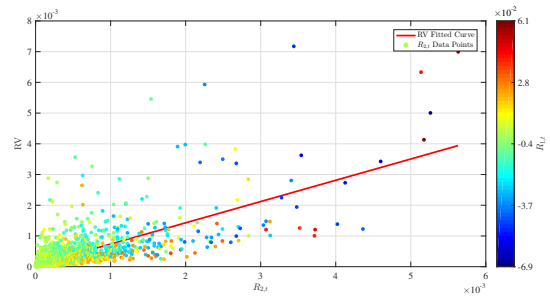


Figure 4 Realized volatility and volatility features

As shown in Figures 3 and 4, the relationship between the realized volatility of the SSE and the trend feature ( $R_{1,t}$ ) as well as the volatility feature ( $R_{2,t}$ ) is illustrated. The red solid line represents the regression results of  $RV_t$  on  $R_{1,t}$  and  $R_{2,t}$ , which are computed as follows:

$$RV_t = \beta_0 + \beta_1 R_{1,t} + \epsilon_t, \quad \text{and} \quad RV_t = \beta_0 + \beta_1 R_{2,t} + \epsilon_t.$$

As shown in Figure 3, the scatter represents the value of  $R_{1,t}$  and the color of the scatter indicates  $R_{2,t}$ . As  $R_{1,t}$  increases to positive values, real volatility decreases rapidly and then stabilizes, and larger values of  $RV_t$  (outliers) appear to correspond to larger values of  $R_{2,t}$  (warmer colors). On the other hand, as shown in Figure 4, the scatter represents  $R_{1,t}$ , with the color changing from blue to red as  $R_{1,t}$  increases. As a weighted sum of squared returns,  $R_{2,t}$  is directly related to market volatility, with realized volatility being a linear function of volatility trend. For a given  $R_{2,t}$ , lower values of  $R_{1,t}$  are usually associated with higher realized volatility.

#### 4.2. Contribution of Path-Dependence to Volatility

To comprehensively evaluate the effectiveness of the path-dependent model in volatility forecasting, different models are introduced and compared to explore the explanatory power of path-dependent models with varying complexity. Specifically, explanatory power is demonstrated by progressively incorporating different path-dependent characteristics. Based on the construction method of path-dependent proposed by Parent (2023), the path-dependent can be formulated in the following basic forms:

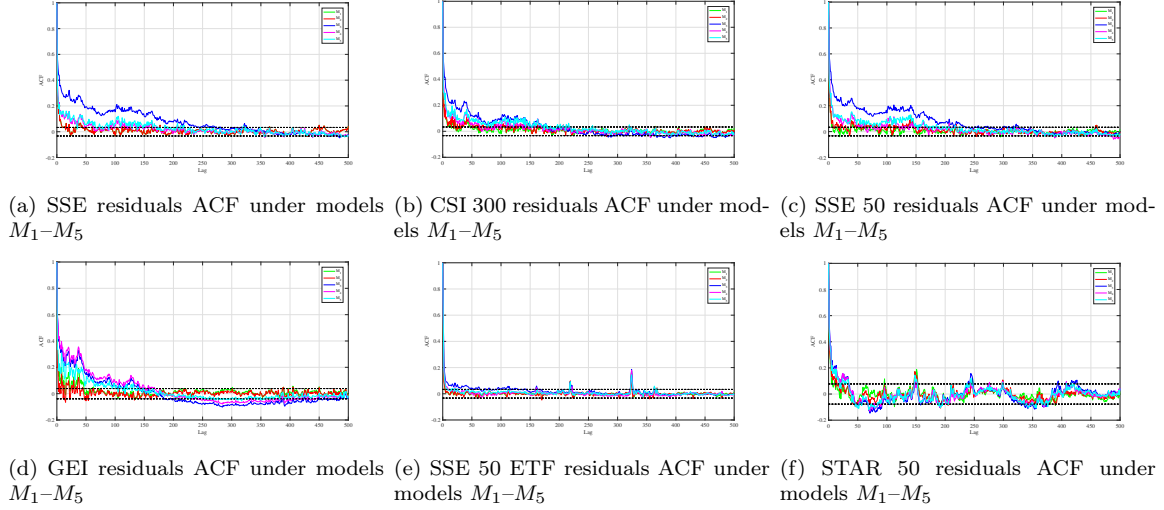


Figure 5 The residuals ACF of each index under model  $M_1-M_5$

$$M_1 : RV_t = \beta_0 + \beta_1 R_{1,t} + \beta_3 \sqrt{R_{2,t}}, \quad (15)$$

$$M_2 : RV_t = \beta_0 + \beta_1 R_{1,t} + \beta_3 R_{2,t}, \quad (16)$$

$$M_3 : RV_t = \beta_0 + \beta_1 R_{1,t}, \quad (17)$$

$$M_4 : RV_t = \beta_0 + \beta_1 |R_{1,t} - \bar{R}_{1,t}|, \quad (18)$$

$$M_5 : RV_t = \beta_0 + \beta_1 R_{1,t}^2. \quad (19)$$

The distinction between model  $M_1$  and model  $M_2$  lies in the nonlinear construction of volatility characteristics. Model  $M_3$  serves as the benchmark model, assessing the explanatory power of a single trend feature on volatility. Model  $M_4$  captures the dispersion of volatility by incorporating the absolute deviation of the trend feature from its mean, reflecting volatility explanatory power in extreme market conditions. Model  $M_5$  emphasizes the direct contribution of the trend feature to volatility.

According to Parent (2022), the dataset is divided into a training set, which comprises 80% of the data from January 4, 2005, to March 13, 2020, and a test set, which consists of the remaining 20% from March 16, 2020, to December 29, 2023.

As shown in Figure 5, it shows the results of the residual autocorrelation of each sample data in the model  $M_1-M_5$  with a lag of 500 items. And the models  $M_1-M_5$  are represented by green, red, blue, magenta, and cyan respectively and the two horizontal lines represent confidence intervals. Taking Figure 5(a) as an example, Model  $M_3$  exhibits strong and persistent autocorrelation in residuals, indicating the presence of unexplained dynamic features in the data, such as nonlinear characteristics, or other factors not captured by the model. In contrast, Model  $M_2$  significantly reduces residual autocorrelation, indicating that the model effectively captures the primary impact of lagged variables on the target variable. As shown in Figures 5(b)– 5(e), model  $M_2$  exhibits a low degree of autocorrelation, with most values falling within the confidence interval. This result indicates that the model  $M_2$  has effectively reduced the unexplained information in the residuals, enhancing overall fitting accuracy and explanatory power. This analysis further confirms that in modeling path-dependent, volatility features play a dominant role in explaining volatility dynamics. This conclusion is consistent with the findings of Parent (2023).

Table 2 Goodness of fit of each index under different models

		SSE		CSI 300		SSE 50		GEI		SSE 50 ETF		STAR 50	
		Train	Test	Train	Test	Train	Test	Train	Test	Train	Test	Train	Test
$M_1$	$R^2$	0.495	0.474	0.455	0.383	0.486	0.442	0.456	0.299	0.175	0.382	0.248	0.059
	RMSE	0.00033	0.00007	0.00035	0.00011	0.00036	0.00009	0.00041	0.00015	0.00084	0.00009	0.00016	0.00016
$M_2$	$R^2$	0.521	0.466	0.503	0.390	0.530	0.391	0.538	0.319	0.206	0.336	0.255	0.0687
	RMSE	0.00032	0.00007	0.00033	0.00010	0.00033	0.00010	0.00034	0.00015	0.00080	0.00010	0.00018	0.00016
$M_3$	$R^2$	0.048	0.044	0.040	0.018	0.0432	0.019	0.0349	0.002	0.000	-0.001	0.0038	0.0259
	RMSE	0.00042	0.00009	0.00105	0.00141	0.00046	0.00012	0.00051	0.00018	0.00096	0.00125	0.00018	0.00019
$M_4$	$R^2$	0.279	0.260	0.255	0.205	0.245	0.257	0.018	0.001	0.0362	0.279	0.091	0.012
	RMSE	0.00046	0.00008	0.00040	0.00015	0.00041	0.00010	0.00054	0.00018	0.00245	0.00080	0.00017	0.00017
$M_5$	$R^2$	0.348	0.200	0.337	0.241	0.390	0.196	0.279	0.103	0.084	0.239	0.163	0.038
	RMSE	0.00043	0.00008	0.00034	0.00012	0.00038	0.00011	0.00043	0.00017	0.00086	0.00012	0.00017	0.00016

Note: all RMSE are retained to five decimal places, and  $R^2$  denotes the goodness-of-fit.

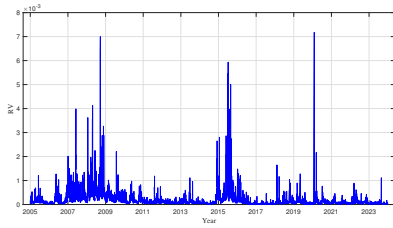


Figure 6 SSE  $RV_t$

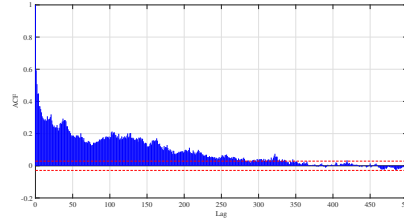


Figure 7 SSE  $RV_t$  ACF

Table 3 Descriptive statistics of realized volatility and other variables

Variables	Mean	Standard Deviation	Skewness	Kurtosis	Maximum	Minimum	ADF	Ljung-Box(10)
RV	0.201	0.399	7.857	95.914	7.175	0.007	-8.798***	7873.7***
CJ	0.849	0.043	16.654	369.009	1.131	0.000	-12.424***	137.6***
CV	0.142	0.243	5.828	55.344	3.898	0.005	-7.314***	11988***
RS <sup>+</sup>	0.099	0.223	14.884	345.431	6.543	0.002	-10.206***	399.7***
RS <sup>-</sup>	0.106	0.248	11.156	220.296	7.079	0.000	-8.979***	3803.4***
REX <sup>+</sup>	0.035	0.076	6.872	76.892	1.447	0.000	-7.619***	6809.6***
REX <sup>-</sup>	0.038	0.083	8.627	111.056	1.546	0.000	-9.561***	6320.3***
REX <sup>m</sup>	0.077	0.132	6.379	71.830	2.556	0.000	-7.341***	12713***
REXQ <sup>+</sup>	0.041	0.081	8.549	114.839	0.002	0.000	-8.857***	5057.1***
REXQ <sup>-</sup>	0.039	0.079	6.930	72.924	1.45	0.000	-7.487***	4623.4***
REXQ <sup>m</sup>	0.069	0.117	6.054	60.071	2.123	0.000	-7.194***	11575***

Note: CV and CJ denote the continuous and jump components, respectively, derived from the underlying volatility model. The Augmented Dickey-Fuller (ADF) test examines the presence of a unit root in the series, with the null hypothesis positing that the series may be non-stationary. The Ljung-Box(10) test evaluates whether time series data exhibit autocorrelation. For ease of presentation, the mean, standard deviation, and maximum values are displayed after multiplying the original values by  $10^3$ . The symbols \*, \*\*, and \*\*\* indicate rejection of the null hypothesis at the 10%, 5%, and 1% significance levels, respectively.



### 4.3. In-sample fitting results

Table 4 Parameter estimation results of the HAR model family

	HAR-RV	HAR-CJ	HAR-RS	HAR-REX	HAR-REQ
$\beta_0$	0.000*** (0.000)	0.000*** (0.000)	0.000*** (0.000)	0.000 (0.000)	0.000 (0.000)
$\beta_1$	0.328*** (0.019)	0.437*** (0.023)	-0.111*** (0.003)	-0.494*** (0.087)	-1.059*** (0.103)
$\beta_2$	0.273*** (0.032)	0.316*** (0.040)	0.814*** (0.054)	1.896*** (0.204)	2.213*** (0.240)
$\beta_3$	0.266*** (0.032)	0.162*** (0.043)	0.014*** (0.096)	1.006*** (0.303)	0.442 (0.379)
$\beta_4$		0.644*** (0.086)	0.001*** (0.024)	-0.492*** (0.098)	0.147 (0.105)
$\beta_5$		-0.198*** (0.209)	1.298*** (0.051)	0.147*** (0.216)	1.326*** (0.240)
$\beta_6$		0.719*** (0.330)	-0.141*** (0.088)	-0.057 (0.344)	-0.644* (0.362)
$\beta_7$				-0.046 (0.081)	0.573*** (0.106)
$\beta_8$				1.325*** (0.166)	0.884*** (0.215)
$\beta_9$				-0.627* (0.242)	-0.060 (0.310)
<i>Adj. R</i> <sup>2</sup>	0.406	0.504	0.581	0.515	0.517

Note: The adjusted  $R^2$  value denotes the adjusted goodness-of-fit. The symbols \*, \*\*, and \*\*\* denote the rejection of the null hypothesis at the 10%, 5%, and 1% significance levels, respectively. The values in parentheses correspond to the standard errors of the respective parameters, with all estimated results rounded to three decimal places.

Using the SSE data as the sample, the selected time period spans from January 4, 2005, to December 29, 2023. After data cleaning, a total of 221,568 five-minute high-frequency observations were obtained.

As illustrated in Figure 6, the time trend of realized volatility from 2005 to 2023 is presented. The vertical axis represents the magnitude of realized volatility, while the horizontal axis denotes the temporal dimension of the data. It is evident from Figure 6 that during the 2008 global financial crisis, the 2016 implementation of China’s first stock market circuit breaker, and the 2020 outbreak of the COVID-19 pandemic, realized volatility exhibited significant peaks, which closely align with the substantial market fluctuations induced by these major events. Figure 7 illustrates the autocorrelation function of volatility, which measures the correlation between different time points in the volatility time series. The autocorrelation structure is distinctly observable, and this characteristic is crucial for developing accurate volatility forecasting models.

To prevent overfitting and further explain the predictive performance of the HAR-PD model family with path dependence, the LASSO method, as described in Section 3.2.1, was employed to construct the HAR-PD model under LASSO<sup>3</sup>.

Table 3 presents the statistical description of volatility based on five-minute high-frequency data, with values of all variables except Ljung-Box(10) test rounded to three decimal places. The distribution of volatility exhibits significant right skewness, indicating a higher frequency of large volatility values. Additionally, the kurtosis value is 95.914, suggesting a highly peaked distribution with fat tails, which implies the potential presence of extreme values. The ADF test statistics for

<sup>3</sup>The specific code can be found at <https://github.com/wangxiaobo018/realized-volatility>

Table 5 Parameter estimation results of the HAR-PD model family

	HAR-PD-RV	HAR-PD-CJ	HAR-PD-RS	HAR-PD-REX	HAR-PD-REQ
$\lambda_1$	39.697*** (0.000)	0.002*** (0.000)	0.367*** (0.000)	0.098*** (0.000)	0.018*** (0.121)
$\lambda_2$		24.225*** (0.000)	15.417*** (0.000)	38.594*** (0.000)	9.616*** (0.000)
$\lambda_3$		14.602*** (0.000)	34.916*** (0.000)	47.169*** (0.000)	0.144*** (0.000)
$\lambda_4$				0.025*** (0.000)	14.832*** (0.000)
$\beta_0$	0.000*** (0.000)	0.000 (0.000)	0.000* (0.000)	0.000*** (0.000)	0.000 (0.000)
$\beta_1$	0.099*** (0.008)	4.848 (2.098)	0.241*** (0.031)	0.587*** (0.110)	1.967*** (0.564)
$\beta_2$	0.533*** (0.019)	-6.487** (2.390)	-0.611** (0.044)	-0.524*** (0.133)	-1.799*** (0.657)
$\beta_3$	0.255*** (0.023)	1.637** (0.720)	0.245*** (0.056)	0.159** (0.047)	-0.104 (0.223)
$\beta_4$		-0.561*** (0.103)	-0.189*** (0.026)	-0.275*** (0.077)	-13.302*** (0.750)
$\beta_5$		1.707*** (0.270)	1.127*** (0.053)	3.467*** (0.167)	12.483*** (0.807)
$\beta_6$		-0.073 (0.466)	-0.144 (0.096)	0.018 (0.272)	0.652* (0.331)
$\beta_7$		0.098 (0.032)	-0.064** (0.020)	0.516*** (0.081)	0.034 (0.103)
$\beta_8$		1.355*** (0.053)	1.593*** (0.051)	2.715*** (0.179)	1.725*** (0.237)
$\beta_9$		-0.026 (0.053)	-0.193* (0.098)	-0.243 (0.300)	-0.987** (0.367)
$\beta_{10}$				-28.388*** (2.906)	0.501*** (0.096)
$\beta_{11}$				26.528*** (2.906)	2.484*** (0.181)
$\beta_{12}$				0.863 (0.685)	-0.690* (0.290)
$Adj.R^2$	0.503	0.509	0.606	0.523	0.537

Note: The adjusted  $R^2$  value denotes the adjusted goodness-of-fit. The symbols \*, \*\*, and \*\*\* denote the rejection of the null hypothesis at the 10%, 5%, and 1% significance levels, respectively. The values in parentheses correspond to the standard errors of the respective parameters, with all estimated results rounded to three decimal places.

Table 6 Sample parameter estimation results for the LASSO-HAR-PD model family

Model	Selected Variable	Parameter Estimate	Standard Deviation	$Adj.R^2$
LASSO-HAR-PD-CJ	$\overline{R}_{2,t-5}$	-1.477*	(0.759)	0.508
	$\overline{R}_{2,t-22}$	1.428*	(0.753)	
	$\overline{PDCJ}_{t-1}$	-0.533***	(0.102)	
	$\overline{PDCJ}_{t-5}$	1.706***	(0.233)	
	$\overline{PDCV}_{t-5}$	1.343***	(0.025)	
LASSO-HAR-PD-RS	$\overline{R}_{2,t-5}$	-3.819***	(0.322)	0.602
	$\overline{R}_{2,t-22}$	3.576***	(0.297)	
	$\overline{PDRS}_{t-1}^+$	-0.136***	(0.025)	
	$\overline{PDRS}_{t-5}^+$	0.973***	(0.046)	
	$\overline{PDRS}_{t-5}^-$	1.073***	(0.038)	
	$\overline{PDRS}_{t-22}^-$	0.264***	(0.064)	
LASSO-HAR-PD-REX	$R_{2,t-1}$	0.791***	(0.156)	0.522
	$\overline{R}_{2,t-5}$	0.282***	(0.020)	
	$\overline{PDREX}_{t-1}^+$	-0.234***	(0.075)	
	$\overline{PDREX}_{t-5}^+$	33.688**	(3.040)	
	$\overline{PDREX}_{t-1}^-$	0.548***	(0.079)	
	$\overline{PDREX}_{t-5}^-$	2.529***	(0.148)	
	$\overline{PDREX}_{t-1}^m$	-34.436***	(3.104)	
	$\overline{PDREX}_{t-5}^m$	33.689***	(3.041)	
LASSO-HAR-PD-REQ	$R_{2,t-1}$	5.456***	(1.389)	0.533
	$\overline{R}_{2,t-5}$	-5.437***	(1.382)	
	$\overline{PDREQ}_{t-1}^+$	-1.388***	(0.228)	
	$\overline{PDREQ}_{t-5}^+$	1.271***	(0.748)	
	$\overline{PDREQ}_{t-5}^-$	-1.900***	(0.194)	
	$\overline{PDREQ}_{t-22}^-$	-1.388**	(0.228)	
	$\overline{PDREQ}_{t-1}^m$	5.303***	(0.073)	
	$\overline{PDREQ}_{t-5}^m$	2.301***	(0.152)	

Note: The adjusted  $R^2$  value denotes the adjusted coefficient of determination. The symbols \*, \*\*, and \*\*\* denote the rejection of the null hypothesis at the 10%, 5%, and 1% significance levels, respectively. The values in parentheses correspond to the standard errors of the respective parameters, with all estimated results rounded to three decimal places.

all variables are negative, and the null hypothesis of a unit root is rejected at the 1% significance level, indicating that all time series variables are stationary. Taking the SSE as an example, Tables 4 and 5 present the parameter estimation results of the HAR and HAR-PD model families. In terms of adjusted  $R^2$ , the HAR-RS model demonstrates the highest adjusted goodness-of-fit among the HAR family models, which is consistent with the volatility prediction model findings reported by Zhang and Zhang (2023). As shown in Table 5, the HAR-PD-RV model exhibits the adjusted  $R^2$  of 0.530, with parameters  $\beta_0$ ,  $\beta_1$ , and  $\beta_2$  being statistically significant at the 1% level, substantially outperforming the baseline HAR-RV model's adjusted  $R^2$  of 0.406. A notable improvement in the adjusted  $R^2$  is also observed when comparing the HAR-CJ model with the HAR-PD-CJ model. The HAR-PD model family demonstrates higher significance levels compared to the baseline HAR model family. The HAR-PD-RS model achieves the highest adjusted  $R^2$  with multiple significant parameters. Similarly, the empirical quantile decomposition-based HAR-PD-REQ model shows superior the adjusted  $R^2$  compared to the baseline HAR-REX model. Overall, the HAR-PD model family consistently demonstrates higher adjusted  $R^2$  values than the HAR model family. Table 6 presents the model variables selected through LASSO, where variables  $R_{2,t-1}$  and  $\bar{R}_{2,t-5}$  were consistently selected across all models in the LASSO-HAR-PD family, further substantiating the contribution of volatility features to the models. The information criterion of the HAR model family and the LASSO-HAR-PD model family shown in the Table 7 shows that a balance has been achieved between the complexity and fit of the LASSO-HAR-PD model family. The improved model does not achieve a better fit by increasing complexity. And the HAR-REQ model constructed by empirical quantiles has smaller AIC and BIC than the HAR-REX model.

Table 7 Information criteria for the HAR and HAR-PD model family

Model	AIC	BIC
HAR-RV	-64062.49	-64030.30
HAR-CJ	-61909.70	-61858.94
HAR-RS	-63022.55	-62971.09
HAR-REX	-62253.74	-62182.94
HAR-REQ	-62468.68	-62193.92
HAR-PD-RV	-62403.08	-62370.92
LASSO-HAR-PD-CJ	-62986.16	-62947.54
LASSO-HAR-PD-RS	-63449.58	-63410.97
LASSO-HAR-PD-REX	-63008.93	-62951.00
LASSO-HAR-PD-REQ	-62823.72	-62759.39

Note: AIC and BIC denote the Akaike information criterion and the Bayesian information criterion, respectively.

#### 4.4. Out-of-sample prediction results

##### 4.4.1. Rolling time window prediction and Out-of-sample prediction evaluation methods

The primary objective of volatility model research is to enhance out-of-sample prediction capabilities. In this study, we employed the Rolling Window Forecasting method to generate predictions for the HAR-PD model family. The specific procedure is outlined as follows:

- (i) The sample data are divided into estimation sample (training sample) and forecast sample (test sample). Following prior studies (Haugom et al., 2014; Feng et al., 2024), forecast sample the length of the forecast sample is generally 300, 600, 1000. In this paper, we will use the forecast sample of length 1000 in the robustness test. After data cleaning, the estimation sample is a fixed window of 4016 days from February 2, 2005, to July 6, 2021, and the forecast sample is the last 600 trading days.
- (ii) Data from  $t = 1, 2, \dots, N = 4295$  was selected as the total sample. In this case, when predicting 1-step into the future, with a fixed window of 4,016 observations ( $H = 4016$ ), the predicted sample is the last 600 days ( $M = 600$ ), similarly when predicting 5-step into the future, the predicted sample is 596 days ( $M = 596$ ), and when predicting 22-step into the future, the predicted sample is 579 days ( $M = 579$ ).
- (iii) The estimated sample intervals are shifted backward with a constant length of the fixed window, and the model's parameters are re-estimated for each backward projection of future volatility to ensure that the sample size used for estimation remains constant.

To comprehensively validate the advantages of the path-dependent structure beyond merely comparing the HAR model family, several researchers (Moreno-Pino and Zohren, 2024; Hansen and Lunde, 2005) have incorporated additional prediction models as baseline comparisons. Thus, in this context, we utilize the GARCH model (Bollerslev, 1986) and its extensions as benchmark models.

Table 8 Out-of-sample forecast loss value of SSE for the future 1-step

Model	MSE	MAE	HMSE	HMAE	QLIKE
GARCH	$1.629 \times 10^{-8}$	$7.912 \times 10^{-5}$	10.468	1.863	-8.364
EGARCH	$1.076 \times 10^{-8}$	$6.422 \times 10^{-5}$	4.666	1.411	-8.545
FGARCH	$8.008 \times 10^{-9}$	$4.967 \times 10^{-5}$	2.135	0.972	-8.578
TGARCH	$8.652 \times 10^{-9}$	$5.605 \times 10^{-5}$	2.511	1.116	-7.741
HAR-RV	$1.284 \times 10^{-8}$	$5.773 \times 10^{-5}$	3.658	0.951	-8.414
HAR-CJ	$1.373 \times 10^{-8}$	$6.976 \times 10^{-5}$	8.679	1.631	-8.409
HAR-RS	$4.427 \times 10^{-9}$	$3.339 \times 10^{-5}$	0.836	0.578	-8.724
HAR-REX	$5.081 \times 10^{-9}$	$3.432 \times 10^{-5}$	0.587	0.552	-8.697
HAR-REQ	$5.056 \times 10^{-9}$	$3.344 \times 10^{-5}$	0.526	0.524	-8.698
HAR-PD-RV	$6.858 \times 10^{-9}$	$3.955 \times 10^{-5}$	0.802	0.574	-8.607
HAR-PD-CJ	$4.693 \times 10^{-9}$	$3.324 \times 10^{-5}$	0.780	0.536	-8.726
HAR-PD-RS	<b><math>4.185 \times 10^{-9}</math></b>	$3.446 \times 10^{-5}$	1.035	0.625	-8.652
HAR-PD-REX	$4.923 \times 10^{-9}$	$3.286 \times 10^{-5}$	0.522	0.511	-8.700
HAR-PD-REQ	$4.855 \times 10^{-9}$	<b><math>3.116 \times 10^{-5}</math></b>	<b>0.450</b>	<b>0.467</b>	-8.707
LASSO-HAR-PD-CJ	$5.038 \times 10^{-9}$	$3.277 \times 10^{-5}$	0.462	0.483	-8.701
LASSO-HAR-PD-RS	$4.391 \times 10^{-9}$	$3.152 \times 10^{-5}$	0.671	0.491	<b>-8.733</b>
LASSO-HAR-PD-REX	$5.022 \times 10^{-9}$	$3.463 \times 10^{-5}$	0.625	0.571	-8.692
LASSO-HAR-PD-REQ	$4.981 \times 10^{-9}$	$3.317 \times 10^{-5}$	0.535	0.520	-8.698

Note: The bold values in the table indicate the minimum under the corresponding loss function, while the underlined values denote the optimal models identified by the MCS test at a significance level of 0.25.

For the evaluation of forecasting accuracy, some scholars, such as [Hyndman and Koehler \(2006\)](#), [Armstrong \(2010\)](#), and [Hansen and Lunde \(2005\)](#), have suggested employing multiple loss functions. In this study, five loss functions are utilized:

$$\begin{aligned}
L_1 : \text{MSE} &= M^{-1} \sum_{m=H+1}^{H+M} (RV_m - \hat{\sigma}_m^2)^2, & L_2 : \text{MAE} &= M^{-1} \sum_{m=H+1}^{H+M} |RV_m - \hat{\sigma}_m^2|, \\
L_3 : \text{HMSE} &= M^{-1} \sum_{m=H+1}^{H+M} \left(1 - \frac{\hat{\sigma}_m^2}{RV_m}\right)^2, & L_4 : \text{HMAE} &= M^{-1} \sum_{m=H+1}^{H+M} \left|1 - \frac{\hat{\sigma}_m^2}{RV_m}\right|, \\
L_5 : \text{QLIKE} &= M^{-1} \sum_{m=H+1}^{H+M} \left\{ \ln(\hat{\sigma}_m^2) + \frac{RV_m}{\hat{\sigma}_m^2} \right\}.
\end{aligned}$$

Here,  $\hat{\sigma}_m^2$  represents the out-of-sample predicted value, while  $RV_m$  denotes the realized market volatility at time  $m$ . Additionally,  $M$  corresponds to the forecasting sample size.

When utilizing the aforementioned loss functions to evaluate model accuracy, relying solely on a single loss function for comparison is insufficient. If the prediction loss of one model is lower than that of another, it is directly concluded that the first model has higher predictive accuracy. However, this judgment is limited and cannot be easily generalized to other datasets or scenarios involving different loss functions. In particular, extreme outliers in the data may significantly impact the calculation of loss functions, potentially leading to misleading evaluations of the volatility model's performance.

Building on this foundation, some scholars ([White, 2000](#); [Diebold and Mariano, 2002](#); [Hansen and Lunde, 2005](#)) have proposed different methods for evaluating the out-of-sample predictive ability of models. However, the most widely applied approach is the MCS method<sup>4</sup>, introduced by [Hansen et al. \(2011\)](#)

#### 4.4.2. Out-of-sample volatility forecasting

Owing to space limitations, the specific results see [Appendix B](#). The MCS test is employed to select the optimal forecasting model at a given confidence level. The MCS test statistics,  $T_R$  and  $T_{max}$ , along with the corresponding  $p$ -values, are obtained through 5000 bootstrap simulations. The MCS procedure is commonly utilized for evaluating sample models. [Table 8](#), presents the optimal models under different loss functions after undergoing the MCS test. As shown in [Table 8](#) the HAR-PD model family exhibits significantly improved predictive performance compared to the HAR model family when forecasting predicting 1-step. Based on the MCS test results, the following conclusions can be drawn:

- (i) As shown in the [Table 8](#), we used CSI 300 as the dataset and used a rolling time window to predict the last 300 days of the dataset. And the predicted loss values of different models (including MSE, MAE, HMSE, HMAE, and QLIKE loss functions) are compared predicting 1-step into the future. In terms of loss values, the HAR-PD family of models performs well in all five loss functions, maintaining low loss values even under LASSO constraints. Notably, the HAR-PD-RS and LASSO-HAR-PD-RS models have significantly lower loss values than the other models for predicting the 1-step, 5-step, and 22-step predictions. In addition, the HAR-REQ model, which defines thresholds based on quantized values, also outperforms the

---

<sup>4</sup>The specific MCS inspection process is shown in the [Appendix A](#).

HAR-REX model. The HAR-PD-REQ model has the lowest loss values under the MAE, HMSE and HMAE loss functions.

- (ii) In comparing the HAR model family and the GARCH model family, found that the prediction accuracy of the HAR model family is higher than that of the GARCH model family, which is consistent with the findings of [Luo and Chen \(2020\)](#). Among the HAR model families, the HAR-RS model has the lowest loss value, while the HAR-CJ model has a better loss value than the HAR-RV model, which is consistent with the findings of [Wen et al. \(2016\)](#).

In summary, the HAR-PD model family demonstrates superior out-of-sample predictive accuracy compared to the HAR model family, further confirming the advantages of volatility forecasting from a path-dependent perspective.

#### 4.5. Robustness testing

In volatility forecasting models, out-of-sample forecasting accuracy is more important than in-sample forecasting accuracy. In order to further validate the forecasting accuracy of the new model, we will conduct a robustness test for out-of-sample forecasting. First, in Section 4.4.2, we adopted various loss functions to evaluate the prediction accuracy of the model based on the MCS test. To further test the robustness of the model, the out-of-sample  $R^2$  test proposed by [Campbell and Thompson \(2008\)](#) will be implemented.

In Section 4.4.1, a rolling window prediction was conducted using the last 600 observations as the prediction sample, following the methodology outlined in [Yang et al. \(2015\)](#). For robustness analysis, a shorter rolling window was selected compared to the out-of-sample forecast, which allowed for a longer prediction interval. To evaluate the model's performance on actual unknown data, this study employed the first 3,616 observations as the rolling window length and the subsequent 1,000 observations as the prediction window. After data cleaning, the estimation sample spanned from January 18, 2005, to November 4, 2019, while the forecast sample covered the period from November 5, 2019, to December 24, 2023.

Secondly in order to assess the model's forecasting ability on other data, new data will be used here for forecasting. Section 4.4.1 uses the SSE, while the robustness test uses 970 days of CSI 300 Index data from January 2, 2020 to December 29, 2023. The data is divided into a 670-day estimation sample from January 2, 2020 to October 11, 2022 and a 300-day forecast sample from October 12, 2022 to December 29, 2023.

Finally, to comprehensively evaluate the superiority of the extended model, additional baseline models were introduced for comparative analysis beyond the basic HAR model family, following the approaches of [Qu et al. \(2018\)](#) and [Moreno-Pino and Zohren \(2024\)](#), who incorporated various traditional baseline models to demonstrate the performance advantages of their extended models.

##### 4.5.1. Out-of-sample $R^2$ test

The out-of-sample  $R^2$  (commonly denoted as  $R_{\text{OOS}}^2(\%)$ ) is used to evaluate the model by comparing the predictive error of the forecasting model with that of the benchmark model. If the model provides better forecasts than the benchmark model, its  $R_{\text{OOS}}^2(\%)$  will be positive. The formula is given as follows:

$$R_{\text{OOS}}^2(\%) = 1 - \frac{\sum_{t=1}^M (\text{RV}_t - \text{RV}_t^j)^2}{\sum_{t=1}^M (\text{RV}_t - \text{RV}_t^0)^2}, \quad j = \text{Model}(1, 2, 3, \dots, 18).$$



Here,  $RV_t$  represents the actual realized volatility,  $RV_t^j$  denotes the out-of-sample predicted value from the forecasting model, and  $RV_t^0$  refers to the out-of-sample predicted value from the benchmark model. If  $R_{\text{OOS}}^2(\%) > 0$ , it indicates that the model's mean squared predictive error (MSPE-adjusted) is lower than that of the benchmark model, demonstrating positive predictive capability. If  $R_{\text{OOS}}^2(\%) = 0$ , the forecasting performance of the model is identical to that of the benchmark model; if  $R_{\text{OOS}}^2(\%) < 0$ , the model performs worse than the benchmark model. The method for calculating the adjusted MSPE is detailed in [Clark and West \(2007\)](#).

#### 4.5.2. Different rolling window lengths

Table 9  $R_{\text{OOS}}^2(\%)$  test results based on a 1,000-day predicting sample

Model	$R_{\text{OOS}}^2(\%)$	MSPE-adjust	$p$ -value
GARCH	-0.172	$3.881 \times 10^{-9}$	0.265
EGARCH	-0.633	$-2.571 \times 10^{-9}$	0.852
FGARCH	-0.625	$-8.033 \times 10^{-9}$	0.868
TGARCH	-0.164	$4.756 \times 10^{-9}$	0.091
HAR-CJ	0.187	$2.154 \times 10^{-8}$	0.084
HAR-RS	0.249	$3.104 \times 10^{-8}$	0.100
HAR-REX	0.187	$2.153 \times 10^{-8}$	0.085
HAR-REQ	0.187	$2.153 \times 10^{-8}$	0.085
HAR-PD-RV	0.255	$2.738 \times 10^{-8}$	0.079
HAR-PD-CJ	0.262	$2.761 \times 10^{-8}$	0.071
HAR-PD-RS	0.256	$3.437 \times 10^{-8}$	0.105
HAR-PD-REX	<b>0.263</b>	$2.636 \times 10^{-8}$	0.062
HAR-PD-REQ	0.259	$2.627 \times 10^{-8}$	0.063
LASSO-HAR-PD-CJ	0.183	$2.140 \times 10^{-8}$	0.085
LASSO-HAR-PD-RS	0.263	$2.632 \times 10^{-8}$	0.061
LASSO-HAR-PD-REX	0.256	$2.732 \times 10^{-8}$	0.065
LASSO-HAR-PD-REQ	0.291	$3.331 \times 10^{-8}$	0.102

Note: Bold values indicate the highest  $R_{\text{OOS}}^2(\%)$  among the models.

As shown in Table 9, all models in the HAR-PD family exhibit an  $R_{\text{OOS}}^2(\%)$  value significantly greater than zero, indicating their strong effectiveness in out-of-sample forecasting. Specifically, when comparing the HAR and HAR-PD model families, the HAR-PD-REX model demonstrates the highest  $R_{\text{OOS}}^2(\%)$  value in out-of-sample forecasting.

Furthermore, in Table 9, the  $R_{\text{OOS}}^2(\%)$  values of the LASSO-HAR-PD model family and HAR-PD model family are also higher than those of the HAR model family, highlighting the overall improvement in predictive accuracy of the HAR-PD model family over traditional HAR model family. These findings further confirm that volatility forecasting models constructed from a path-dependence perspective exhibit superior predictive accuracy compared to baseline models.

#### 4.5.3. Different sample data

In Table 10, the loss function values for the future 1-step predictions indicate that the HAR-REQ and HAR-PD-REQ models exhibit lower loss values across two different loss functions, while the HAR-PD-RS model achieves the lowest loss value under the QLIKE loss function. Notably, the

Table 10 Out-of-sample forecast loss value of CSI 300 for the future 1-step

Model	MSE	MAE	HMSE	HMAE	QLIKE
GARCH	$1.117 \times 10^{-8}$	$5.326 \times 10^{-5}$	1.922	0.853	-8.441
EGARCH	$2.444 \times 10^{-8}$	$1.216 \times 10^{-4}$	11.766	2.556	-8.115
FGARCH	$1.701 \times 10^{-8}$	$7.235 \times 10^{-5}$	5.397	1.361	-8.414
TGARCH	$1.478 \times 10^{-8}$	$7.028 \times 10^{-5}$	4.267	1.277	-7.865
HAR-RV	$1.228 \times 10^{-8}$	$5.466 \times 10^{-5}$	3.409	0.865	-8.364
HAR-CJ	$8.565 \times 10^{-9}$	$3.831 \times 10^{-5}$	0.477	0.496	-8.536
HAR-RS	$7.919 \times 10^{-9}$	$3.905 \times 10^{-5}$	1.003	0.571	-8.553
HAR-REX	$9.162 \times 10^{-9}$	$4.421 \times 10^{-5}$	0.800	0.666	-8.513
HAR-REQ	$8.866 \times 10^{-9}$	$3.818 \times 10^{-5}$	<b>0.433</b>	<b>0.484</b>	-8.525
HAR-PD-RV	$9.513 \times 10^{-9}$	$4.577 \times 10^{-5}$	1.241	0.731	-8.501
hHAR-PD-CJ	$8.422 \times 10^{-9}$	$4.226 \times 10^{-5}$	0.688	0.604	-8.529
HAR-PD-RS	$7.774 \times 10^{-9}$	$3.886 \times 10^{-5}$	1.771	0.574	<b>-8.555</b>
HAR-PD-REX	$8.064 \times 10^{-9}$	$4.062 \times 10^{-5}$	0.640	0.593	-8.535
HAR-PD-REQ	$7.740 \times 10^{-9}$	$3.956 \times 10^{-5}$	0.602	0.569	-8.554
LASSO-HAR-PD-CJ	$8.427 \times 10^{-9}$	$4.250 \times 10^{-5}$	0.703	0.612	-8.528
LASSO-HAR-PD-RS	<b><math>7.638 \times 10^{-9}</math></b>	<b><math>3.757 \times 10^{-5}</math></b>	0.956	0.590	-8.597
LASSO-HAR-PD-REX	$7.741 \times 10^{-9}$	$3.951 \times 10^{-5}$	0.599	0.567	-8.553
LASSO-HAR-PD-REQ	$8.283 \times 10^{-9}$	$4.140 \times 10^{-5}$	0.647	0.600	-8.526

Note: The bold values in the table indicate the minimum under the corresponding loss function, while the underlined values denote the optimal models identified by the MCS test at a significance level of 0.25.

proposed HAR-REQ model and its improved HAR-PD-REQ variant outperform other models in volatility forecasting under the MAE, HMSE, and HMAE loss functions.

## 5. Conclusion

This study systematically investigated volatility modeling and forecasting based on high-frequency data. First, an innovative approach to modeling and forecasting volatility from a path-dependence perspective was proposed. Specifically, the fundamental theory of path-dependent was introduced, and in combination with other foundational volatility decomposition theories, a more flexible and accurate volatility model was constructed. Furthermore, a new volatility model was developed from the path dependence perspective to enhance the in-sample fitting and predictive capabilities of mainstream HAR model families. In a high-frequency data environment, the incorporation of path-dependent features allows the new model to better capture the dynamic behavior of stock market volatility. The construction process of the new model is described in detail, including its mathematical formulation, parameter estimation methods, and theoretical analysis.

To validate the effectiveness of the new model, an empirical analysis was conducted using five-minute high-frequency trading data from the SSE. Various evaluation methods and testing techniques were employed to comprehensively assess the new model, including in-sample fitting, out-of-sample

forecasting, rolling window evaluation, and multiple statistical tests. The results indicated that the HAR-PD model family demonstrated superior predictive performance across all evaluations.

In out-of-sample forecasting, the HAR-PD model family, constructed based on path dependence, consistently outperformed the original HAR model family, significantly improving prediction accuracy. This result remained significant across different datasets, indicating the strong robustness of the new model. Notably, under the rolling window and out-of-sample evaluation methods, the new model exhibited sustained superiority. It is worth mentioning that among all models examined in this study, the HAR-PD-RS model achieved the highest prediction accuracy in forecasting daily volatility, while the HAR-PD-REQ model demonstrated superior predictive capability in medium- and long-term (5-step and 22-step) volatility forecasting.

In conclusion, the HAR-PD model family constructed in this study offers new possibilities for capturing the complexity of stock market volatility. The volatility model, developed by integrating the HAR model family with a path-dependence perspective, significantly enhances the accuracy and reliability of volatility forecasting. The findings of this study not only enrich the theoretical literature on volatility modeling but also provide valuable tools for practical applications, aiding investors and risk managers in better understanding and forecasting market fluctuations. Since the HAR model family and the HAR-PD model family lack sufficient ability to capture the nonlinear fluctuation characteristics in high-frequency data, our subsequent research will focus on improving the nonlinear prediction performance of such models.

## References

- F. Black, M. Scholes, The pricing of options and corporate liabilities, *Journal of political economy* 81 (1973) 637–654.
- B. Dupire, et al., Pricing with a smile, *Risk* 7 (1994) 18–20.
- S. L. Heston, A closed-form solution for options with stochastic volatility with applications to bond and currency options, *The review of financial studies* 6 (1993) 327–343.
- P. Foschi, A. Pascucci, Path dependent volatility, *Decisions in Economics and Finance* 31 (2008) 13–32.
- C. Fulvio, R. Roberto, Discrete-time volatility forecasting with persistent leverage effect and the link with continuous-time volatility modeling, *Journal of Business & Economic Statistics* 30 (2012) 368–380.
- L. Parent, Rough path-dependent volatility models, Available at SSRN 4270481 (2022).
- O. E. Euch, M. Rosenbaum, Perfect hedging in rough heston models, *The Annals of Applied Probability* 28 (2018) 3813–3856.
- J. Guyon, J. Lekeufack, Volatility is (mostly) path-dependent, *Quantitative Finance* 23 (2023) 1221–1258.
- R. F. Engle, Autoregressive conditional heteroscedasticity with estimates of the variance of united kingdom inflation, *Econometrica* 50 (1982) 987–1007.
- L. R. Glosten, R. Jagannathan, D. E. Runkle, On the relation between the expected value and the volatility of the nominal excess return on stocks, *The Journal of Finance* 48 (1993) 1779–1801.

- M. Haas, S. Mittnik, M. S. Paoletta, A new approach to markov-switching garch models, *Journal of Financial Econometrics* 2 (2004) 493–530.
- D. Creal, S. J. Koopman, A. Lucas, Generalized autoregressive score models with applications, *Journal of Applied Econometrics* 28 (2013) 777–795.
- T. G. Andersen, T. Bollerslev, Answering the skeptics: Yes, standard volatility models do provide accurate forecasts, *International Economic Review* 39 (1998) 885–905.
- F. Corsi, A Simple Approximate Long-Memory Model of Realized Volatility, *Journal of Financial Econometrics* 7 (2009) 174–196.
- S. S. Lee, P. A. Mykland, Jumps in financial markets: A new nonparametric test and jump dynamics, *The Review of Financial Studies* 21 (2008) 2535–2563.
- A. J. Patton, S. Kevin, Good Volatility, Bad Volatility: Signed Jumps and The Persistence of Volatility, *The Review of Economics and Statistics* 97 (2015) 683–697.
- Barndorff-Nielsen, K. Silja, S. Neil, Measuring downside risk-realised semivariance, *CREATES Research Paper* (2008).
- A. Clements, H. Rodrigo, Moderate and extreme volatility: Do the magnitude of returns matter for forecasting?, Available at SSRN 3443259 (2019).
- P. R. Hansen, A. Lunde, J. M. Nason, The model confidence set, *Econometrica* 79 (2011) 453–497.
- J. Y. Campbell, S. B. Thompson, Predicting excess stock returns out of sample: Can anything beat the historical average?, *The Review of Financial Studies* 21 (2008) 1509–1531.
- N. Ning, J. Wu, Well-Posedness and Stability Analysis of Two Classes of Generalized Stochastic Volatility Models 12 (2021) 79–109.
- A. Cozma, C. Reisinger, Strong convergence rates for euler approximations to a class of stochastic path-dependent volatility models, *SIAM Journal on Numerical Analysis* 56 (2018) 3430–3458.
- O. E. Barndorff-Nielsen, N. Shephard, Power and bipower variation with stochastic volatility and jumps, *Journal of Financial Econometrics* 2 (2004) 1–37.
- O. E. Barndorff-Nielsen, N. Shephard, Realized power variation and stochastic volatility models, *Bernoulli* 9 (2003) 243–265.
- X. Huang, G. Tauchen, The relative contribution of jumps to total price variance, *Journal of Financial Econometrics* 3 (2005) 456–499.
- T. G. Andersen, T. Bollerslev, F. X. Diebold, Roughing it up: Including jump components in the measurement, modeling, and forecasting of return volatility, *The Review of Economics and Statistics* 89 (2007) 701–720.
- F. Corsi, R. Reno, HAR volatility modelling with heterogeneous leverage and jumps, Available at SSRN 1316953 (2009).
- Y. Ding, D. Kambouroudis, D. G. McMillan, Forecasting realised volatility: Does the lasso approach outperform har?, *Journal of International Financial Markets, Institutions and Money* 74 (2021) 101386.

- F. Audrino, S. D. Knaus, Lassoing the har model: A model selection perspective on realized volatility dynamics, *Econometric Reviews* 35 (2016) 1485–1521.
- R. Tibshirani, Regression shrinkage and selection via the lasso, *Journal of the Royal Statistical Society Series B: Statistical Methodology* 58 (1996) 267–288.
- K. P. Burnham, D. R. Anderson, Multimodel inference: understanding AIC and BIC in model selection, *Sociological Methods & Research* 33 (2004) 261–304.
- Y. Aït-Sahalia, P. A. Mykland, L. Zhang, How often to sample a continuous-time process in the presence of market microstructure noise, *The Review of Financial Studies* 18 (2005) 351–416.
- L. Zhang, P. A. Mykland, Y. Aït-Sahalia, A tale of two time scales: Determining integrated volatility with noisy high-frequency data, *Journal of the American Statistical Association* 100 (2005) 1394–1411.
- F. Corsi, S. Mittnik, C. Pigorsch, U. Pigorsch, The volatility of realized volatility, *Econometric Reviews* 27 (2008) 46–78.
- L. Parent, Investigating approaches to modeling rough path-dependent volatility: Insights and implications, Available at SSRN 4579759 (2023).
- Y.-J. Zhang, H. Zhang, Volatility forecasting of crude oil futures market: Which structural change-based har models have better performance?, *International Review of Financial Analysis* 85 (2023) 102454.
- E. Haugom, H. Langeland, P. Molnár, S. Westgaard, Forecasting volatility of the US oil market, *Journal of Banking & Finance* 47 (2014) 1–14.
- Y. Feng, Y. Zhang, Y. Wang, Out-of-sample volatility prediction: Rolling window, expanding window, or both?, *Journal of Forecasting* 43 (2024) 567–582.
- F. Moreno-Pino, S. Zohren, Deepvol: Volatility forecasting from high-frequency data with dilated causal convolutions, *Quantitative Finance* 24 (2024) 1105–1127.
- P. R. Hansen, A. Lunde, A forecast comparison of volatility models: does anything beat a garch(1,1)?, *Journal of Applied Econometrics* 20 (2005) 873–889.
- T. Bollerslev, Generalized autoregressive conditional heteroskedasticity, *Journal of Econometrics* 31 (1986) 307–327.
- R. J. Hyndman, A. B. Koehler, Another look at measures of forecast accuracy, *International Journal of Forecasting* 22 (2006) 679–688.
- J. S. Armstrong, Long-range forecasting, 2nd, Available at SSRN 666990 (2010).
- H. White, A reality check for data snooping, *Econometrica* 68 (2000) 1097–1126.
- F. X. Diebold, R. S. Mariano, Comparing predictive accuracy, *Journal of Business & Economic Statistics* 20 (2002) 134–144.
- J. Luo, L. Chen, Realized volatility forecast with the bayesian random compressed multivariate har model, *International Journal of Forecasting* 36 (2020) 781–799.

- F. Wen, X. Gong, S. Cai, Forecasting the volatility of crude oil futures using har-type models with structural breaks, *Energy Economics* 59 (2016) 400–413.
- K. Yang, L. Chen, F. Tian, Realized volatility forecast of stock index under structural breaks, *Journal of Forecasting* 34 (2015) 57–82.
- H. Qu, Q. Duan, M. Niu, Modeling the volatility of realized volatility to improve volatility forecasts in electricity markets, *Energy Economics* 74 (2018) 767–776.
- T. E. Clark, K. D. West, Approximately normal tests for equal predictive accuracy in nested models, *Journal of Econometrics* 138 (2007) 291–311.

## Appendix A. The procedure of MCS test

The MCS testing procedure is as follows:

- (i) Given the existence of  $m_0 = 18$  distinct volatility forecasting models, these models collectively form the set  $M_0$ , defined as  $M_0 = 1, 2, \dots, m_0$ . Each model provides daily market volatility estimates for the subsequent  $M$  days, denoted as  $\hat{\sigma}_m^2$  ( $m = H+1, \dots, H+M$ ). Based on the five loss functions defined in this study ( $L_1, L_2, \dots, L_5$ ), the loss function value for each prediction is computed as  $L_{i,j,m}$ , where  $i = 1, 2, \dots, 5$ ;  $j = 1, 2, \dots, m_0$ ; and  $m = H+1, \dots, H+M$ . For any two models  $u$  and  $v$  ( $u, v \in M_0$ ), their relative loss function value is calculated as  $d_{i,uv,m} = L_{i,u,m} - L_{i,v,m}$ .
- (ii) A superior model set  $M^*$  is defined as A superior model set  $M^*$  is defined as:

$$M^* \equiv \{u \in M_0 : \mathbb{E}(d_{i,uv,m}) \leq 0, \text{ for all } v \in M_0\}$$

The MCS testing process involves conducting a series of significance tests within the set  $M_0$  to eliminate models with inferior predictive ability. In each test iteration, the null hypothesis assumes that the two models possess identical predictive ability, expressed as:  $H_0, M : \mathbb{E}(d_{i,uv,m}) = 0, \text{ for all } u, v \in M \subset M_0$ .

- (iii) Model selection is conducted using the equivalence test  $\delta_M$  and the elimination rule  $e_M$ . Initially, the null hypothesis  $H_0 : M = M_0$  is proposed. At a significance level  $\alpha$ , the equivalence test  $\delta_M$  is applied to test  $H_0, M$ . If the null hypothesis is not rejected, then  $M_{1-\alpha}^* = M$  is defined. Otherwise, the elimination rule  $e_M$  is employed to remove rejected models from  $M$ . This process continues until no further rejection of the null hypothesis occurs, ultimately yielding the surviving models under the MCS procedure.

There are typically two types of test statistics used in the MCS evaluation: the range statistic  $T_R$  and the semiquadratic statistic  $T_{\max}$ , which are defined as follows:

$$T_R = \max_{u,v \in M} \frac{|\bar{d}_{i,uv}|}{\sqrt{\text{var}(\bar{d}_{i,uv})}}, \quad T_{\max} = \max_{u,v \in M} \frac{\bar{d}_{i,uv}^2}{\text{var}(\bar{d}_{i,uv})}$$

where  $\bar{d}_{i,uv} = M^{-1} \sum_{m=H+1}^{H+M} d_{i,uv,m}$  represents the average loss value between model  $u$  and model  $v$ . The  $T_R$  and  $T_{\max}$  statistics, along with their corresponding  $p$ -values, are obtained using the Bootstrap method.

## Appendix B. Out-of-sample forecast loss value and MCS test



Table B.11 MCS test for the future 1-step volatility forecasting model of the SSE

Model	QLIKE $_{\alpha_1}$		MSE $_{\alpha_1}$		QLIKE $_{\alpha_2}$		MSE $_{\alpha_2}$		QLIKE $_{\alpha_3}$		MSE $_{\alpha_3}$	
	$T_{max}$	$T_R$	$T_{max}$	$T_R$	$T_{max}$	$T_R$	$T_{max}$	$T_R$	$T_{max}$	$T_R$	$T_{max}$	$T_R$
GARCH	0.000	0.000	0.019	0.045	0.034	0.029	0.000	0.000	0.000	0.000	0.000	0.000
EGARCH	0.000	0.000	0.099	0.013	0.000	0.000	0.000	0.000	0.000	0.000	0.000	0.000
FGARCH	0.000	0.000	0.964	0.029	0.000	0.000	0.000	0.000	0.000	0.000	0.000	0.000
TGARCH	0.000	0.000	0.013	0.000	0.000	0.000	0.000	0.000	0.000	0.000	0.000	0.000
HAR-RV	0.000	0.000	0.235	0.120	0.000	0.000	0.000	0.000	0.000	0.000	0.000	0.000
HAR-CJ	0.000	0.000	0.183	0.525	0.000	0.000	0.000	0.000	0.000	0.000	0.000	0.000
HAR-RS	1.000	0.000	1.000	0.465	1.000	0.000	1.000	0.324	1.000	0.000	0.944	0.319
HAR-REX	0.075	0.525	1.000	0.574	0.000	0.000	1.000	0.423	0.000	0.000	0.958	0.412
HAR-REQ	0.391	0.679	1.000	1.000	1.000	1.000	0.243	0.000	0.000	0.000	1.000	1.000
HAR-PD-RV	0.000	0.000	1.000	0.485	0.000	0.000	0.102	0.099	0.000	0.000	0.000	0.000
HAR-PD-CJ	0.712	0.705	1.000	1.000	0.000	1.000	0.802	1.000	1.000	0.827	0.499	1.000
HAR-PD-RS	0.984	0.005	1.000	1.000	0.470	0.248	1.000	1.000	1.000	1.000	1.000	1.000
HAR-PD-REX	1.000	0.994	1.000	<b>1.000</b>	0.661	0.436	<b>1.000</b>	<b>1.000</b>	0.000	0.000	<b>1.000</b>	<b>1.000</b>
HAR-PD-REQ	1.000	1.000	1.000	1.000	1.000	1.000	1.000	1.000	0.000	0.000	1.000	1.000
LASSO-HAR-PD-CJ	0.657	0.679	1.000	1.000	0.274	1.000	0.971	0.440	1.000	1.000	0.998	0.977
LASSO-HAR-PD-RS	<b>1.000</b>	<b>1.000</b>	<b>1.000</b>	1.000	<b>1.000</b>	<b>1.000</b>	1.000	1.000	<b>1.000</b>	<b>1.000</b>	0.997	1.000
LASSO-HAR-PD-REX	0.993	0.705	1.000	1.000	0.306	0.243	1.000	1.000	0.474	1.000	1.000	1.000
LASSO-HAR-PD-REQ	0.037	0.001	1.000	1.000	0.000	0.000	1.000	1.000	0.000	0.000	1.000	1.000

Note:  $\alpha_1$ ,  $\alpha_2$  and  $\alpha_3$  denote that the significance level of MCS test is taken as 0.01, 0.1 and 0.25, respectively. The  $p$  value indicates the prediction accuracy of the model, and is retained to three decimal places; the higher the  $p$  value, the better the prediction accuracy. The optimal model under the test is bolded to indicate that the model has the optimal volatility prediction performance in the corresponding prediction interval.

Table B.12 MCS test for the future 5-step volatility forecasting model of the SSE

Model	QLIKE $_{\alpha_1}$		MSE $_{\alpha_1}$		QLIKE $_{\alpha_2}$		MSE $_{\alpha_2}$		QLIKE $_{\alpha_3}$		MSE $_{\alpha_3}$	
	$T_{max}$	$T_R$	$T_{max}$	$T_R$	$T_{max}$	$T_R$	$T_{max}$	$T_R$	$T_{max}$	$T_R$	$T_{max}$	$T_R$
GARCH	0.000	0.000	0.000	0.000	0.034	0.029	0.000	0.000	0.000	0.000	0.000	0.000
EGARCH	0.000	0.000	0.099	0.013	0.000	0.000	0.000	0.000	0.000	0.000	0.000	0.000
FGARCH	0.000	0.000	0.964	0.029	0.000	0.000	0.000	0.000	0.000	0.000	0.000	0.000
TGARCH	0.000	0.000	0.047	0.067	0.000	0.000	0.000	0.000	0.000	0.000	0.000	0.000
HAR-RV	0.000	0.000	0.278	0.079	0.000	0.000	0.000	0.000	0.000	0.000	0.000	0.000
HAR-CJ	0.227	0.996	1.000	0.453	0.000	0.000	1.000	0.423	0.000	0.000	0.993	0.408
HAR-RS	1.000	0.006	1.000	0.095	1.000	0.000	1.000	0.085	1.000	0.000	0.906	0.089
HAR-REX	0.138	0.622	1.000	0.946	0.000	0.000	1.000	0.423	0.000	0.000	0.868	0.462
HAR-REQ	0.656	1.000	0.246	0.453	0.237	0.640	1.000	1.000	1.000	1.000	1.000	1.000
HAR-PD-RV	0.000	0.000	1.000	0.485	0.000	0.000	0.107	0.097	0.000	0.000	0.000	0.000
HAR-PD-CJ	0.867	1.000	1.000	1.000	1.000	1.000	0.802	1.000	0.339	0.573	1.000	1.000
HAR-PD-RS	0.946	0.004	1.000	1.000	0.665	0.640	1.000	1.000	0.557	0.512	1.000	1.000
HAR-PD-REX	1.000	1.000	1.000	<b>1.000</b>	1.000	<b>1.000</b>	1.000	<b>1.000</b>	0.845	0.983	<b>1.000</b>	<b>1.000</b>
HAR-PD-REQ	1.000	1.000	<b>1.000</b>	1.000	1.000	1.000	1.000	1.000	1.000	0.000	1.000	1.000
LASSO-HAR-PD-CJ	0.769	1.000	1.000	1.000	0.345	0.995	0.971	0.440	0.263	0.512	0.995	1.000
LASSO-HAR-PD-RS	<b>1.000</b>	<b>1.000</b>	1.000	1.000	<b>1.000</b>	1.000	1.000	1.000	<b>1.000</b>	<b>1.000</b>	0.993	1.000
LASSO-HAR-PD-REX	0.995	1.000	1.000	1.000	0.644	0.640	<b>1.000</b>	1.000	0.484	0.554	1.000	1.000
LASSO-HAR-PD-REQ	0.053	0.004	1.000	1.000	0.000	0.000	1.000	1.000	0.000	0.000	0.748	1.000

Note:  $\alpha_1$ ,  $\alpha_2$  and  $\alpha_3$  denote that the significance level of MCS test is taken as 0.01, 0.1 and 0.25, respectively. The  $p$  value indicates the prediction accuracy of the model, and is retained to three decimal places; the higher the  $p$  value, the better the prediction accuracy. The optimal model under the test is bolded to indicate that the model has the optimal volatility prediction performance in the corresponding prediction interval.

Table B.13 MCS test for the future 22-step volatility forecasting model of the SSE

Model	QLIKE $_{\alpha_1}$		MSE $_{\alpha_1}$		QLIKE $_{\alpha_2}$		MSE $_{\alpha_2}$		QLIKE $_{\alpha_3}$		MSE $_{\alpha_3}$	
	$T_{max}$	$T_R$	$T_{max}$	$T_R$	$T_{max}$	$T_R$	$T_{max}$	$T_R$	$T_{max}$	$T_R$	$T_{max}$	$T_R$
GARCH	0.019	0.045	0.000	0.000	0.034	0.029	0.000	0.000	0.000	0.000	0.000	0.000
EGARCH	0.000	0.000	0.099	0.013	0.000	0.000	0.000	0.000	0.000	0.000	0.000	0.000
FGARCH	0.000	0.000	0.964	0.029	0.000	0.000	0.000	0.000	0.000	0.000	0.000	0.000
TGARCH	0.113	0.034	0.047	0.067	0.000	0.000	0.000	0.000	0.000	0.000	0.000	0.000
HAR-RV	0.122	0.125	0.278	0.079	0.000	0.000	0.000	0.000	0.000	0.000	0.000	0.000
HAR-CJ	1.000	0.660	1.000	0.453	0.000	0.000	0.990	0.559	0.000	0.000	0.993	0.559
HAR-RS	1.000	0.415	1.000	0.095	1.000	0.002	0.972	0.359	0.000	0.000	0.972	0.359
HAR-REX	1.000	0.573	1.000	0.946	0.000	0.000	0.816	0.481	0.000	0.000	0.816	0.481
HAR-REQ	1.000	0.937	0.246	0.453	0.123	0.513	1.000	0.878	0.000	0.000	1.000	0.877
HAR-PD-RV	0.971	0.124	1.000	0.485	0.000	0.000	0.000	0.000	0.000	0.000	0.000	0.000
HAR-PD-CJ	1.000	0.750	1.000	1.000	0.303	0.548	1.000	0.672	0.000	0.000	1.000	0.652
HAR-PD-RS	1.000	0.998	1.000	1.000	0.797	0.003	1.000	0.997	0.000	0.000	1.000	0.997
HAR-PD-REX	1.000	<b>1.000</b>	1.000	0.914	0.995	<b>1.000</b>	<b>1.000</b>	<b>1.000</b>	0.000	0.000	<b>1.000</b>	<b>1.000</b>
HAR-PD-REQ	<b>1.000</b>	0.995	<b>1.000</b>	<b>1.000</b>	1.000	1.000	1.000	0.985	0.000	0.000	1.000	0.985
LASSO-HAR-PD-CJ	0.000	0.000	1.000	1.000	0.259	0.513	0.996	0.615	0.000	0.000	0.995	0.978
LASSO-HAR-PD-RS	1.000	0.990	1.000	1.000	<b>1.000</b>	1.000	1.000	0.978	<b>1.000</b>	<b>1.000</b>	0.993	0.978
LASSO-HAR-PD-REX	1.000	0.987	1.000	1.000	0.604	0.548	1.000	1.000	0.000	0.000	1.000	0.971
LASSO-HAR-PD-REQ	0.000	0.000	1.000	1.000	0.000	0.000	0.612	0.621	0.000	0.000	0.612	0.621

Note:  $\alpha_1$ ,  $\alpha_2$  and  $\alpha_3$  denote that the significance level of MCS test is taken as 0.01, 0.1 and 0.25, respectively. The  $p$  value indicates the prediction accuracy of the model, and is retained to three decimal places; the higher the  $p$  value, the better the prediction accuracy. The optimal model under the test is bolded to indicate that the model has the optimal volatility prediction performance in the corresponding prediction interval.

Table B.14 Out-of-sample forecast loss value of SSE for the future 5-step

Model	MSE	MAE	HMSE	HMAE	QLIKE
GARCH	$1.636 \times 10^{-8}$	$7.935 \times 10^{-5}$	10.693	1.872	-8.360
EGARCH	$1.174 \times 10^{-8}$	$6.927 \times 10^{-5}$	5.059	1.511	-8.499
FGARCH	$1.364 \times 10^{-8}$	$7.432 \times 10^{-5}$	6.299	1.696	-8.467
TGARCH	$9.072 \times 10^{-9}$	$4.660 \times 10^{-5}$	1.102	0.711	-6.626
HAR-RV	$1.292 \times 10^{-8}$	$5.798 \times 10^{-5}$	3.682	0.954	-8.412
HAR-CJ	$5.085 \times 10^{-9}$	$3.364 \times 10^{-5}$	0.521	0.518	-8.700
HAR-RS	$4.453 \times 10^{-9}$	$3.351 \times 10^{-5}$	0.840	0.580	-8.724
HAR-REX	$5.113 \times 10^{-9}$	$3.444 \times 10^{-5}$	0.590	0.554	-8.696
HAR-REQ	$5.087 \times 10^{-9}$	$3.353 \times 10^{-5}$	0.527	0.524	-8.697
HAR-PD-RV	$6.902 \times 10^{-9}$	$3.966 \times 10^{-5}$	0.805	0.575	-8.606
HAR-PD-CJ	$5.062 \times 10^{-9}$	$3.257 \times 10^{-5}$	<b>0.445</b>	0.474	-8.699
HAR-PD-RS	$4.209 \times 10^{-9}$	$3.460 \times 10^{-5}$	1.039	0.627	-8.659
HAR-PD-REX	$4.954 \times 10^{-9}$	$3.294 \times 10^{-5}$	0.525	0.519	-8.700
HAR-PD-REQ	$4.888 \times 10^{-9}$	<b><u><math>3.127 \times 10^{-5}</math></u></b>	0.454	<b>0.468</b>	-8.707
LASSO-HAR-PD-CJ	$5.072 \times 10^{-9}$	$3.287 \times 10^{-5}$	0.464	0.484	-8.700
LASSO-HAR-PD-RS	<b><u><math>4.417 \times 10^{-9}</math></u></b>	$3.162 \times 10^{-5}$	0.673	0.493	<b><u>-8.732</u></b>
LASSO-HAR-PD-REX	$5.013 \times 10^{-9}$	$3.325 \times 10^{-5}$	0.536	0.521	-8.698
LASSO-HAR-PD-REQ	$5.053 \times 10^{-9}$	$3.473 \times 10^{-5}$	0.627	0.572	-8.692

Note: The bold values in the table indicate the minimum under the corresponding loss function, while the underlined values denote the optimal models identified by the MCS test at a significance level of 0.25.

Table B.15 Out-of-sample forecast loss value of SSE for the future 22-step

Model	MSE	MAE	HMSE	HMAE	QLIKE
GARCH	$1.687 \times 10^{-8}$	$8.075 \times 10^{-5}$	8.872	1.842	-8.379
EGARCH	$1.226 \times 10^{-8}$	$7.551 \times 10^{-5}$	7.940	1.822	-8.378
FGARCH	$1.927 \times 10^{-8}$	$1.113 \times 10^{-4}$	15.470	2.887	-8.299
TGARCH	$1.082 \times 10^{-8}$	$4.808 \times 10^{-5}$	0.314	0.473	-6.994
HAR-RV	$1.284 \times 10^{-8}$	$5.694 \times 10^{-5}$	3.708	0.950	-8.437
HAR-CJ	$5.082 \times 10^{-9}$	$3.311 \times 10^{-5}$	0.525	0.519	-8.710
HAR-RS	$4.413 \times 10^{-9}$	$3.282 \times 10^{-5}$	0.846	0.578	-8.736
HAR-REX	$5.119 \times 10^{-9}$	$3.396 \times 10^{-5}$	0.594	0.554	-8.707
HAR-REQ	$5.099 \times 10^{-9}$	$3.308 \times 10^{-5}$	0.529	0.524	-8.708
HAR-PD-RV	$6.986 \times 10^{-9}$	$3.955 \times 10^{-5}$	0.817	0.578	-8.614
HAR-PD-CJ	$5.062 \times 10^{-9}$	$3.204 \times 10^{-5}$	0.446	0.474	-8.710
HAR-PD-RS	<b><math>4.213 \times 10^{-9}</math></b>	$3.422 \times 10^{-5}$	1.059	0.630	-8.669
HAR-PD-REX	$4.964 \times 10^{-9}$	$3.253 \times 10^{-5}$	0.525	0.510	-8.711
HAR-PD-REQ	$4.944 \times 10^{-9}$	$3.102 \times 10^{-5}$	<b><u>0.459</u></b>	<b><u>0.470</u></b>	<b><u>-8.717</u></b>
LASSO-HAR-PD-CJ	$5.068 \times 10^{-9}$	$3.232 \times 10^{-5}$	0.464	0.483	-8.711
LASSO-HAR-PD-RS	<u><math>4.377 \times 10^{-9}</math></u>	<b><u><math>3.097 \times 10^{-5}</math></u></b>	0.677	0.491	-8.744
LASSO-HAR-PD-REX	$5.020 \times 10^{-9}$	$3.277 \times 10^{-5}$	0.535	0.519	-8.709
LASSO-HAR-PD-REQ	$5.081 \times 10^{-9}$	$3.438 \times 10^{-5}$	0.632	0.574	-8.702

Note: The bold values in the table indicate the minimum under the corresponding loss function, while the underlined values denote the optimal models identified by the MCS test at a significance level of 0.25.

Table B.16 MCS test for each volatility model of CSI 300 with a forecast sample of 300-day

Model	$H = 1$				$H = 5$				$H = 22$			
	QLIKE		MSE		QLIKE		MSE		QLIKE		MSE	
	$T_{max}$	$T_R$	$T_{max}$	$T_R$	$T_{max}$	$T_R$	$T_{max}$	$T_R$	$T_{max}$	$T_R$	$T_{max}$	$T_R$
GARCH	0.000	0.000	0.000	0.000	0.034	0.029	0.000	0.000	0.000	0.000	0.000	0.000
EGARCH	0.000	0.000	0.121	0.214	0.000	0.000	0.000	0.000	0.000	0.000	0.000	0.000
FGARCH	0.000	0.000	0.964	0.029	0.000	0.000	0.000	0.000	0.000	0.000	0.000	0.000
TGARCH	0.000	0.000	0.047	0.067	0.000	0.000	0.000	0.000	0.000	0.000	0.000	0.000
HAR-RV	0.000	0.000	0.278	0.079	0.000	0.000	0.000	0.000	0.000	0.000	0.000	0.000
HAR-CJ	1.000	0.991	1.000	0.985	0.000	0.000	0.990	0.559	0.000	0.000	0.993	0.559
HAR-RS	1.000	0.991	1.000	1.000	1.000	0.002	0.972	0.359	0.000	0.000	0.972	0.359
HAR-REX	0.000	0.000	1.000	0.448	0.000	0.000	0.816	0.481	0.000	0.000	0.816	0.481
HAR-REQ	1.000	1.000	1.000	0.985	0.123	0.513	1.000	0.878	0.000	0.000	1.000	0.877
HAR-PD-RV	0.000	0.000	0.974	0.929	0.000	0.000	0.000	0.000	0.000	1.000	0.851	0.000
HAR-PD-CJ	0.392	0.540	1.000	1.000	0.303	0.548	1.000	0.672	0.000	0.000	1.000	0.652
HAR-PD-RS	<b>1.000</b>	<b>1.000</b>	0.989	0.985	0.797	0.003	1.000	0.997	0.000	0.000	1.000	0.997
HAR-PD-REX	1.000	1.000	1.000	0.985	0.995	<b>1.000</b>	<b>1.000</b>	<b>1.000</b>	0.000	0.000	<b>1.000</b>	<b>1.000</b>
HAR-PD-REQ	1.000	1.000	<b>1.000</b>	1.000	1.000	1.000	1.000	0.985	0.000	0.000	1.000	0.985
LASSO-HAR-PD-CJ	0.317	0.502	<b>1.000</b>	0.191	0.259	0.513	0.996	0.615	0.000	0.000	0.995	0.978
LASSO-HAR-PD-RS	<b>1.000</b>	<b>1.000</b>	0.997	0.864	<b>1.000</b>	1.000	1.000	0.978	<b>1.000</b>	<b>1.000</b>	0.993	0.978
LASSO-HAR-PD-REX	0.370	0.557	1.000	0.864	0.604	0.548	1.000	1.000	0.000	0.000	1.000	0.971
LASSO-HAR-PD-REQ	1.000	0.927	<b>1.000</b>	<b>1.000</b>	0.000	0.000	0.612	0.621	0.000	0.000	0.612	0.621

Note: The above are the results of MCS test at the confidence level of 0.25. The  $p$ -value indicates the prediction accuracy of the model, and is retained to three decimal places; the higher the  $p$ -value, the better the prediction accuracy. The largest  $p$  value is marked in bold to indicate that the model has the optimal volatility prediction performance in the corresponding prediction interval.

Table B.17 Out-of-sample forecast loss value of CSI 300 for the future 5-step

Model	MSE	MAE	HMSE	HMAE	QLIKE
GARCH	$1.201 \times 10^{-8}$	$5.525 \times 10^{-5}$	2.226	0.905	-8.428
EGARCH	$1.806 \times 10^{-8}$	$7.424 \times 10^{-5}$	4.124	1.348	-8.410
FGARCH	$2.555 \times 10^{-8}$	$1.236 \times 10^{-4}$	10.718	2.559	-8.207
TGARCH	$1.065 \times 10^{-8}$	$4.545 \times 10^{-5}$	0.873	0.680	-8.173
HAR-RV	$1.286 \times 10^{-8}$	$5.516 \times 10^{-5}$	3.669	0.878	-8.367
HAR-CJ	$9.018 \times 10^{-9}$	$3.846 \times 10^{-5}$	0.476	0.497	-8.543
HAR-RS	$7.581 \times 10^{-9}$	<b><math>3.795 \times 10^{-5}</math></b>	0.832	0.552	-8.514
HAR-REX	$9.645 \times 10^{-9}$	$4.461 \times 10^{-5}$	0.807	0.671	-8.519
HAR-REQ	$9.352 \times 10^{-9}$	<u><math>3.840 \times 10^{-5}</math></u>	<b>0.433</b>	<b>0.485</b>	-8.531
HAR-PD-RV	$9.985 \times 10^{-9}$	$4.602 \times 10^{-5}$	1.257	0.736	-8.507
HAR-PD-CJ	$8.873 \times 10^{-9}$	$4.258 \times 10^{-5}$	0.696	0.611	-8.533
HAR-PD-RS	<u><math>7.575 \times 10^{-9}</math></u>	$3.907 \times 10^{-5}$	0.948	0.583	-8.541
HAR-PD-REX	$8.502 \times 10^{-9}$	$4.152 \times 10^{-5}$	0.662	0.607	-8.540
HAR-PD-REQ	$8.179 \times 10^{-9}$	$4.040 \times 10^{-5}$	0.632	0.585	<u>-8.559</u>
LASSO-HAR-PD-CJ	$8.878 \times 10^{-9}$	$4.282 \times 10^{-5}$	0.712	0.619	-8.533
LASSO-HAR-PD-RS	$7.576 \times 10^{-9}$	$3.907 \times 10^{-5}$	0.948	0.581	-8.542
LASSO-HAR-PD-REX	$8.745 \times 10^{-9}$	$4.247 \times 10^{-5}$	0.682	0.618	-8.531
LASSO-HAR-PD-REQ	$8.182 \times 10^{-9}$	$4.034 \times 10^{-5}$	0.629	0.583	-8.558

Note: The bold values in the table indicate the minimum under the corresponding loss function, while the underlined values denote the optimal models identified by the MCS test at a significance level of 0.25.

Table B.18 Out-of-sample forecast loss value of CSI 300 for the future 22-step

Model	MSE	MAE	HMSE	HMAE	QLIKE
GARCH	$1.254 \times 10^{-8}$	$5.804 \times 10^{-5}$	1.002	1.022	-8.449
EGARCH	$2.051 \times 10^{-8}$	$7.835 \times 10^{-5}$	8.450	1.641	-8.417
FGARCH	$7.790 \times 10^{-8}$	$2.627 \times 10^{-4}$	5.054	1.369	-8.414
TGARCH	$1.071 \times 10^{-8}$	$4.048 \times 10^{-5}$	0.656	0.589	-8.178
HAR-RV	$1.264 \times 10^{-8}$	$5.235 \times 10^{-5}$	3.818	0.886	-8.417
HAR-CJ	$9.098 \times 10^{-9}$	$3.647 \times 10^{-5}$	0.483	0.498	-8.590
HAR-RS	$7.613 \times 10^{-9}$	$3.638 \times 10^{-5}$	0.814	0.553	-8.575
HAR-REX	$9.566 \times 10^{-9}$	$4.221 \times 10^{-5}$	0.800	0.668	-8.567
HAR-REQ	$9.380 \times 10^{-9}$	<b><math>3.599 \times 10^{-5}</math></b>	<b>0.434</b>	<b>0.482</b>	-8.583
HAR-PD-RV	$9.664 \times 10^{-9}$	$4.243 \times 10^{-5}$	1.269	0.732	-8.557
HAR-PD-CJ	$9.071 \times 10^{-9}$	$4.154 \times 10^{-5}$	0.766	0.635	-8.577
HAR-PD-RS	<b><math>7.625 \times 10^{-9}</math></b>	$3.705 \times 10^{-5}$	0.941	0.574	-8.599
HAR-PD-REX	$8.751 \times 10^{-9}$	$4.087 \times 10^{-5}$	0.716	0.629	-8.592
HAR-PD-REQ	$8.536 \times 10^{-9}$	$4.077 \times 10^{-5}$	0.752	0.627	<b><u>-8.601</u></b>
LASSO-HAR-PD-CJ	$9.075 \times 10^{-9}$	$4.177 \times 10^{-5}$	0.782	0.643	-8.577
LASSO-HAR-PD-RS	$8.176 \times 10^{-9}$	$3.687 \times 10^{-5}$	0.724	0.559	-8.597
LASSO-HAR-PD-REX	$9.124 \times 10^{-9}$	$4.334 \times 10^{-5}$	0.790	0.667	-8.570
LASSO-HAR-PD-REQ	$8.556 \times 10^{-9}$	$4.080 \times 10^{-5}$	0.750	0.625	-8.600

Note: The bold values in the table indicate the minimum under the corresponding loss function, while the underlined values denote the optimal models identified by the MCS test at a significance level of 0.25.